Published in final edited form as:
Pflugers Arch. 2014 July ; 466(7): 1301–1316. doi:10.1007/s00424-013-1362-5.

Dual depolarization responses generated within the same lateral septal neurons by TRPC4-containing channels

Jinbin Tian,
Department of Integrative Biology and Pharmacology, University of Texas Health Science Center at Houston, 6431 Fannin St. MSB4.128, Houston, TX 77030, USA

Dhananjay P. Thakur,
Department of Integrative Biology and Pharmacology, University of Texas Health Science Center at Houston, 6431 Fannin St. MSB4.128, Houston, TX 77030, USA

Yungang Lu,
Department of Integrative Biology and Pharmacology, University of Texas Health Science Center at Houston, 6431 Fannin St. MSB4.128, Houston, TX 77030, USA

Yingmin Zhu,
Department of Integrative Biology and Pharmacology, University of Texas Health Science Center at Houston, 6431 Fannin St. MSB4.128, Houston, TX 77030, USA

Marc Freichel,
Department of Pharmacology, Heidelberg University, 69120 Heidelberg, Germany

Veit Flockerzi, and
Experimental and Clinical Pharmacology and Toxicology, Saarland University, 66421 Homburg, Germany

Michael X. Zhu
Department of Integrative Biology and Pharmacology, University of Texas Health Science Center at Houston, 6431 Fannin St. MSB4.128, Houston, TX 77030, USA

Michael X. Zhu: Michael.X.Zhu@uth.tmc.edu

Abstract

In the central nervous system, canonical transient receptor potential (TRPC) channels have been implicated in mediating neuronal excitation induced by stimulating metabotropic receptors, including group 1 metabotropic glutamate receptors (mGluRs). Lateral septal (LS) neurons express high levels of TRPC4 and group I mGluRs. However, to what extent native TRPC4-containing channels (TRPC4-cc) are activated as well as the impact of different levels of TRPC4-cc activation on neuronal excitability remain elusive. Here, we report that stimulating LS neurons with group I mGluR agonist, (*S*)-3,5-DHPG, causes either an immediate increase in firing rate or an initial burst followed by a pause of firing, which can be correlated with below-threshold-

Correspondence to: Michael X. Zhu, Michael.X.Zhu@uth.tmc.edu.

Conflict of interest Authors declare no conflict of interest.

depolarization (BTD) or above-threshold-plateau-depolarization (ATPD), respectively, in whole-cell recordings. The early phase of BTD and the entire ATPD are completely absent in neurons from TRPC4$^{-/-}$ mice. Moreover, in the same LS neurons, BTD can be converted to ATPD at more depolarized potentials or with a brief current injection, suggesting that BTD and ATPD may represent partial and full activations of TRPC4-cc, respectively. We show that coincident mGluR stimulation and depolarization is required to evoke strong TRPC4-cc current, and Na^+ and Ca^{2+} influx, together with dynamic changes of intracellular Ca^{2+}, are essential for ATPD induction. Our results suggest that TRPC4-cc integrates metabotropic receptor stimulation with intracellular Ca^{2+} signals to generate two interconvertible depolarization responses to affect excitability of LS neurons in distinct fashions.

Keywords

Cation channel; Excitability; Glutamate receptor

Introduction

The canonical transient receptor potential (TRPC) family of cation channels consists of seven members, TRPC1–TRPC7. According to sequence similarities, TRPC members are further classified into three subgroups: TRPC1/C4/C5, TRPC2, and TRPC3/C6/C7 [37]. Although all TRPCs are found in the central nervous system (CNS), TRPC4 and TRPC5 are more broadly distributed [8, 19]. It has been suggested that functional TRPC4 channels are either homomeric or heteromeric tetramers [1, 3, 5] and in neurons TRPC4 likely forms heteromeric channels with TRPC1, TRPC5, or both [12, 23, 34, 35].

Whereas most brain areas express comparable levels of TRPC4 and C5 [4, 8], the lateral septal (LS) nucleus expresses much more TRPC4 than TRPC5 and other TRPC isoforms [8]. Therefore, it has been suggested that the majority of TRPC channels in these neurons are either homomeric TRPC4 or heteromeric TRPC1/C4 channels [23], both of which we refer to as TRPC4-containing channels (TRPC4-cc) in the current study. Moreover, the majority of LS neurons are mid-sized, spiny-shaped, GABAergic neurons [10, 32]. As such, TRPC4-cc may execute relatively consistent functions across all LS neurons, making them ideal candidates to study activation mechanisms and functional implications of native TRPC4-cc in the CNS.

Numerous studies have provided evidence that TRPC channels are receptor-operated, Ca^{2+}-permeable, nonselective cation channels [1, 25, 26]. In neurons from multiple brain regions, including prefrontal cortex, hippocampus, hypothalamus, entorhinal cortex, and lateral septum, TRPC4-cc and the closely related TRPC5 have been shown to be activated following stimulation of G protein-coupled receptors (GPCRs), including metabotropic glutamate receptors (mGluRs) [6, 8, 23, 24], muscarinic acetylcholine receptors [39], and serotonin receptors [20, 27]. Notably, two types of membrane potential changes have been described following GPCR-mediated TRPC4-cc activation in these neurons. The first exhibits a low amplitude but long-lasting depolarization [6, 8, 33], whereas the second displays a rapid high-amplitude depolarization typically containing burst firing, which is

then followed by a plateau depolarization associated with few or no action potentials [23, 39]. It was, however, unclear whether the two types of membrane potential changes are mediated by the same or different channels and what mechanisms or conditions lead to the occurrence of these distinct responses.

Here, we examined TRPC4-cc activation and membrane potential responses in LS neurons from mouse brain slices by whole-cell patch clamp recording of individual neurons under multiple stimulation paradigms. We show that depending on activity levels, Ca^{2+} influx and intracellular Ca^{2+} dynamics, TRPC4-cc activation through mGluRs elicits two interconvertible depolarizing responses characterized by below-threshold-depolarization (BTD) and above-threshold-plateau-depolarization (ATPD), which lead to distinct response patterns in LS neuron firing activities.

Methods

Animals and brain slice preparation

Wild-type (C57BL/6) and TRPC4 knockout ($TRPC4^{-/-}$, in C57BL/6 background) [9] mice (P21-P60, M/F) were anesthetized by isoflurane before they were sacrificed following procedures in accordance with NIH guidelines and approved by the Animal Welfare Committee of the University of Texas Health Science Center at Houston. Whole brain was excised quickly and immediately immersed into ice-cold cutting solution consisting of (in mM): 60 NaCl, 110 sucrose, 28 $NaHCO_3$, 7 $MgSO_4$, 3 KCl, 1.25 NaH_2PO_4, 0.5 $CaCl_2$, and 0.6 Na ascorbate, bubbled with 95 % O_2 + 5 % CO_2, until the brain tissue was chilled completely. The forebrain was blocked and mounted to prechilled cutting stage of Leica VT1200S vibratome. Coronal slices (350 μm) were sectioned sequentially in the ice-cold cutting solution. Slices containing septal nuclei were transferred and incubated in normal artificial cerebrospinal fluid (aCSF) consisting of (in mM): 125 NaCl, 26 $NaHCO_3$, 1 $MgSO_4$, 2.5 KCl, 1.25 NaH_2PO_4, 2 $CaCl_2$, and 10 glucose, bubbled with 95 % O_2 + 5 % CO_2, at 35 °C for at least 90 min before recording. The choline-Cl aCSF contained choline-Cl in place of NaCl of the normal aCSF. The nominally Ca^{2+}-free aCSF was made by omitting $CaCl_2$ from the normal aCSF.

Drug delivery

Each brain slice placed in the recording chamber (Warner Instruments) was continuously perfused with the normal aCSF unless indicated otherwise. Drugs were diluted in aCSF and applied either through whole-chamber perfusion or by pressure ejection through a drug-delivery glass pipette positioned about 5–20 μm away from the target cell upstream of the aCSF flow (Fig. 1(A)). The puffs were delivered by Toohey Spritzer Pressure System IIe (Toohey Company) with the trigger controlled via stimulation protocols programmed using PatchMaster software (HEKA Instruments). The puff duration was 30 ms and the air pressure ranged 5–30 psi. The recording chamber was continuously perfused with aCSF during the drug ejection.

(*S*)-3,5-Dihydroxyphenylglycine (DHPG), YM298198, 2-methyl-6-(phenylethynyl)pyridine hydrochloride (MPEP), and nifedipine were purchased from Abcam Biochemicals.

SKF96365 and tetrodotoxin were purchased from Tocris Bioscience. 1,2-Bis(2-aminophenoxy)ethane-*N*,*N*,*N*′,*N*′-tetraacetic acid (BAPTA) was obtained from Sigma-Aldrich. ML204 was kindly provided by Dr. Xuechuan Hong (Wuhan University).

Electrophysiology

Glass pipettes (Sutter Instrument) were pulled using a Narishige PC-10 puller. Loose patches were made using recording pipettes with resistance of 1–3 MΩ, when filled with normal aCSF. After reaching the target cell, the positive pressure within the recording pipette was released and gentle suction applied until the seal resistance reached and stabilized between 30 and 100 MΩ, which usually took a few minutes. During this time, current was monitored for the occurrence of downward deflections, which indicate spontaneous firing. The current was continuously monitored for at least 5 min to ensure that amplitude of spike discharges was stable. After that, the pipette offset was adjusted to zero before recording initiated in voltage-clamp mode with the holding potential set at 0 mV.

Whole-cell patch clamp recordings were made using pipettes with tip resistance of 3–6 MΩ when filled with the intracellular solution containing (in mM): 130 K-methanesulfonate, 7 KCl, 0.05 EGTA, 1 Na_2-ATP, 3 Mg-ATP, 0.05 Na_2-GTP, and 10 HEPES, with pH adjusted to 7.3 by KOH and osmolarity of 300 mOsm. LS neurons were visualized using a ×60 water objective lens and infrared-differential interference contrast-videomicroscopy (Olympus BX51WI with OLY-150IR video camera). When not being stimulated or tested, the LS neuron was voltage clamped at −70 mV. The temperature of the recording chamber was maintained at approximately 32 °C by passing the perfusion solution (aCSF) through an in-line heater (Warner Instrument) at 3 ml/min driven by a Rabbit™ peristaltic pump (Rainin Instrument).

Membrane potential (V_m) was measured in current clamp mode when current injection value was set to zero. Resting V_m was defined as the median between action potential threshold and the maximum after-hyperpolarization potential for neurons that fired action potentials, and as the mean membrane potential value for neurons that were silent. Cells with resting V_m values less negative than −40 mV were excluded.

Following the measurements of V_m, the LS neuron was sequentially recorded using five stimulation/recording protocols. For the first three protocols, the cell was held at either −70 or −45 mV in either current or voltage clamp mode (namely CC-70, VC-70, and CC-45) while DHPG or other drugs were puffed at the preprogrammed time point. Current clamp with the initial potential of −70 mV (CC-70) allowed observation of drug-elicited membrane potential changes in the absence of spontaneous firing while that with the initial potential of −45 mV (CC-45) revealed effects of the drug on firing activity of the neuron. The voltage clamp at −70 mV (VC-70) allowed recording of drug-elicited currents. After recordings using the above three protocols, the cell was held at −80 mV in current clamp mode and was given successive 20-ms current pulse injections starting from 200 pA with a 100-pA increment until it reached 1 nA. The interval between each current pulse was 1.3 s and the ejection of DHPG was triggered at the end of each current injection (see Fig. 4(Aa)). This protocol is named CC-80s. Finally, a VC-70s protocol was applied, in which the cell was voltage-clamped at −70 mV. A 50-ms step to −45 mV was first applied to inactivate voltage-

gated Na^+ channels. This was followed by a step to −10 mV for 200 ms to activate voltage-gated Ca^{2+} channels (VGCCs) and drug ejection was triggered at the beginning of the step to −10 mV (see Fig. 6(Ca)). To examine the temporal relationship between DHPG application and depolarization, the drug ejection time was set to initiate at different times before and after the start of the step pulse to −10 mV and the step duration at −10 mV was also varied as indicated (see Fig. 9). The CC-80s and VC-70s protocols were designed to assess the effect of activation of voltage-gated Na^+ and/or Ca^{2+} channels on the drug-evoked responses.

Data acquisition and analysis

Data were acquired using an EPC10 amplifier operated by PatchMaster software (both from HEKA). Recordings were filtered at 3 kHz and digitized at 10 kHz. The amplitude and time-to-peak of maximal depolarization were measured at the point where the depolarization reached the first peak, excluding action potentials, following DHPG stimulation. The area-under-the-trace was measured as the integral of individual CC-80s recording traces between the first point following current injection and the last point of the trace. Among the nine traces obtained from the CC-80s recordings, only the one with the maximal integral value was selected to represent the maximal depolarization elicited by the drug(s). With the VC-70s protocol, the maximal inward current was measured as the first negative peak following repolarization to −70 mV. Firing frequency was calculated as spikes per second within the specified ranges of CC-45 recordings. All measurements were made off-line using the analysis functions of the PatchMaster software. Representative traces in figures were reproduced in Igor Pro (Wavemetrics). Student's *t* test was used to compare the mean values of two groups of measurements. Repeated two-way ANOVA analysis followed by Newman–Keuls post hoc tests were used to compare firing frequency changes between wild-type and $TRPC4^{-/-}$ groups. Data are presented as means±SEM. Differences were considered to be statistically significant when $P < 0.05$.

Results

Two distinct response patterns of firing activities elicited by brief pressure ejection of mGluR agonist onto LS neurons and its dependence on TRPC4

The group 1 mGluRs is coupled to $G_{q/11}$-phospholipase C (PLC) signaling pathway, which is well known to trigger TRPC channel activation [1, 25, 26]. A previous study has shown that whole-chamber perfusion of a group I mGluR agonist, either 30 μM DHPG or 30 μM 1S, 3R-ACPD, to the rat or mouse brain slice elicited repetitive membrane potential oscillations and extended depolarization lasting for about 1–5 s in the LS neurons [23]. The long-term and whole-chamber application of the mGluR agonist mimics pathological conditions of excitatory neuronal death associated with wide spread network elevation of glutamate. This configuration also exposes all neuronal components in the brain slice to the drug such that the detected response does not necessarily represent the direct action of the mGluR agonist on the neuron being studied. To examine immediate, largely direct responses of single LS neurons to mGluR activation, which should resemble the physiological conditions when glutamate spillover is limited to synaptic regions of few cells, we ejected DHPG (30 μM) toward the soma of the recorded LS neuron via a nearby puff pipette (Fig.

1(A)). Individual LS neurons were randomly selected from all subdivisions of the LS nucleus in mouse brain slices, with a slightly higher percentage of cells from the dorsal lateral regions (Fig. 1(B)). With loose-patch recordings of spontaneously firing LS neurons, which should not disrupt the intracellular content, we detected two distinct patterns of firing changes in response to a brief (30 ms) pressure ejection of DHPG. About 36 % of neurons (4 out of 11) responded to DHPG with an increased firing rate without a pause (Fig. 1 (Cb)), while the rest (64 %, 7 out of 11) displayed a long pause (0.5–2 s) before firing resumed at an increased rate (Fig. 1(Cc)). As a control, ejecting the buffer (aCSF) alone did not cause any change in the firing rate (Fig. 1(Ca)), suggesting that these neurons were not sensitive to mechanical effect of the ejection.

To examine the mechanism underlying the two distinct response patterns on excitability of LS neurons evoked by DHPG, we used whole-cell patch clamp configuration in subsequent experiments. With the solution compositions shown in “Methods,” the mean resting V_m of all recorded LS neurons was −56.6±0.5 mV (n = 162). The cells were current clamped at either −70 mV (CC-70) or −45 mV (CC-45) while DHPG was applied by pressure ejection. With cells clamped at −45 mV, 87 % (58/67) wild-type (WT) LS neurons fired action potentials spontaneously. The remaining 13 % neurons remained silent during the 55-s recording period (Fig. 2(D), *left*). Whereas ejecting aCSF did not change V_m and firing patterns of LS neurons (Fig. 2(Aa)), ejecting 30 μM DHPG elicited two distinct types of membrane potential responses and accompanied firing pattern changes that resembled those seen with the loose-patch recordings. Among the firing LS neurons, 31 % (18/58) showed small gradual baseline depolarization that reached the peak(4.3±0.7mV) within 1.13±0.16 s, which then gradually declined (Fig. 2(Ab, F)). Accompanied with the depolarization, the firing frequency also increased (Fig. 2 (Ab)). By contrast, the other 69 % cells responded to DHPG ejection with a short burst followed by a plateau depolarization of, on average, 40.2±1.1 mV (Fig. 2(Ac,d, F)). During the plateau depolarization, there was a momentary pause of firing, which was then followed by robust firing for a short period of time (Fig. 2(Ac,d)). The plateau depolarization matches approximately the pause duration measured with the loose patch and explains the baseline deflection detected in such recordings (e.g., see Fig. 1(Cc)). Evidently, the plateau depolarization was strong enough to inactivate voltage-gated Na^+ channels, suppressing the generation of action potentials. It is interesting to note that this firing pattern also occurred spontaneously without any experimental stimulation in about 3 % (5 out of 162 recorded) LS neurons recorded under whole-cell conditions (see Fig. 2(B) for an example), suggesting that the response to DHPG ejection resembles, to some extent, naturally occurring physiological activity of LS neurons. Therefore, results from the whole-cell recordings faithfully reproduced those obtained from loose patches and suggested that the difference in the level of membrane depolarization underlay the two distinct response patterns of LS neuron firing in response to DHPG ejection.

Remarkably, in brain slices prepared from TRPC4$^{-/-}$ mice, LS neurons exhibited a totally different response pattern to DHPG ejection as compared to WT. Although DHPG ejection also evoked depolarization in TRPC4$^{-/-}$ LS neurons, the depolarization amplitude was small and it occurred very slowly (Fig. 2(C, F, G)). During the first 2 s immediately after DHPG

ejection, WT neurons either exhibited a progressive increase in firing frequency (Fig. 2(Ab, H)) or burst firing followed by plateau depolarization with pause of firing (Fig. 2(Ac,d)). By contrast, the firing frequency of TRPC4$^{-/-}$ LS neurons either remained unchanged (four out of nine neurons) or showed an obvious decrease (five out of nine, similar to the example in Fig. 2(C)) during the same time period (Fig. 2(H)). The firing frequency of TRPC4$^{-/-}$ LS neurons only increased at a much later time, which correlated with the slow time course of depolarization in these neurons (Fig. 2(C, G)). These data suggest that both the early phase of small depolarization and the entire plateau depolarization, as well as the accompanied firing pattern changes, required the presence of TRPC4. This raised the possibility that TRPC4-cc might mediate two distinct types of depolarization responses to mGluR stimulation, with different outcomes on LS neuron excitability.

As shown in Fig. 2(E), the levels of membrane depolarization elicited by DHPG are clearly segregated between the two groups of WT LS neurons, as if a “threshold” is present for the occurrence of plateau depolarization. In order to better distinguish these two types of depolarizing responses, we categorized the small depolarization as BTD and the large plateau depolarization as ATPD. BTD is accompanied with an increase in firing frequency whereas ATPD causes a pause of firing for 1.9±0.3 s despite the initial burst and the subsequent high frequency firing. As shown in Fig. 2(F and G), although WT BTD neurons had similar depolarization amplitude as TRPC4$^{-/-}$ LS neurons, the BTD neurons reached the peak much faster than TRPC4$^{-/-}$ ones.

BTD and ATPD evoked by ejecting mGluR agonist onto non-firing LS neurons

As can be seen from Fig. 2(D), although 13 % (9/67) WT LS neurons did not fire action potentials at CC-45, the mean amplitude of depolarization evoked by DHPG ejection of these non-firing neurons was similar to that of firing neurons. Interestingly, the two neurons that showed small depolarization (BTD) were clearly segregated from those that exhibited strong depolarization (ATPD). The percentage of ATPD neurons for the non-firing cells (∼78 %) was comparable to that of firing ones (∼69 %), indicating that spontaneous firing was not essential for the induction of ATPD.

To gain further insights of DHPG-induced depolarization under non-firing conditions, all LS neurons were also recorded when being current clamped at −70 mV (CC-70). Again, ejecting aCSF barely caused any membrane potential change (Fig. 3(Aa)), while 30 μM DHPG caused two distinct types of depolarization (Fig. 3(Ab, Ac)), which were clearly segregated in the amplitude distribution histogram (Fig. 3(C)). BTD (41/76, 54 %) was characterized by a small but long-lasting depolarization averaging 4.8±0.5 mVat the first peak (Fig. 3(Ab, C, D)), while ATPD exhibited a strong plateau depolarization averaging 55.2±1.8 mV, which typically contained an initial fast rise to positive potentials with burst firing, followed by a plateau depolarization with or without associated action potentials (Fig. 3(Ac, Ad, C, D)).

Similar to the results of CC-45, at CC-70, LS neurons from TRPC4$^{-/-}$ mice only showed small depolarization that had similar mean amplitude as WT BTD, but with longer time-to-peak period (Fig. 3(B, D, E)). TRPC4$^{-/-}$ LS neurons never showed ATPD in response DHPG ejection. The complete absence of ATPD in TRPC4$^{-/-}$ LS neurons provides strong

evidence that TRPC4-cc is required for the plateau depolarization evoked by pressure ejection of 30 μM DHPG onto the somata of WT LS neurons. The significant difference in the rate of reaching the first peak of depolarization between TRPC4$^{-/-}$ and WT BTD neurons suggests that TRPC4-cc also contributes to the initial depolarization evoked by the mGluR agonist in the BTD neurons, but a TRPC4-independent mech-anism(s) is also present for the slower and moderate depolarization elicited by DHPG in the LS neurons.

Compared to the CC-45 recording, a lower percentage of cells responded to DHPG stimulation with ATPD (46 %) and the time-to-peak period of BTD appeared longer at CC-70. These results indicate that at potentials more negative than V_m, less LS neurons can respond to DHPG ejection onto the somata with ATPD, but the general response patterns are similar to cells held at −45 mV.

Effect of current injection on mGluR-mediated TRPC4-cc activation

It was previously shown in sharp electrode intracellular recordings that brief depolarizing current injection immediately evoked prolonged TRPC1/C4-mediated plateau depolarization in LS neurons continuously perfused with 1S, 3R-ACPD or DHPG [23]. Therefore, we tested the extent to which current injection could facilitate the membrane potential response induced by ejection of DHPG onto LS neurons. Cells were current-clamped at −80 mV. A series of nine episodes of brief (20 ms) injections of increasing positive charge at 100-pA increments were applied immediately preceding the pressure ejection of DHPG, and membrane potential changes were recorded for 1.3 s during each episode (Fig. 4(Aa), designated as CC-80s protocol). In the absence of drug ejection or with the ejection of aCSF onto the somata of LS neurons, current injections caused depolarization and burst firing that were restricted to the time period of the injection pulse (Fig. 4(Ab)). However, ejecting 30 μM DHPG immediately following the current injection evoked ATPD of variable durations long after the ejection had stopped in 83 % (62/75) of WT LS neurons (Fig. 4(Ac, D)). Notably, not every current step elicited ATPD in the same neuron and the size of ATPD (measured by area under the trace) was highly variable among different steps in the same neuron. The maximal ATPD could occur at any step of the series (Fig. 4(Ac inset)). Therefore, the size of ATPD was correlated with neither the amount of injected current nor the number of repetitive DHPG ejections, suggesting that both the induction and maintenance of ATPD were highly dynamic. Interestingly, in six ATPD neurons, plateau depolarization did not develop immediately after DHPG ejection but appeared after the membrane potential had completely recovered from the injection-elicited depolarization. This type of response, which we referred to as delayed-PD (Fig. 4(Ae)), further supports the highly dynamic nature of ATPD induction and also suggests that ATPD is not a direct consequence of current injection. Also notable was that the amplitude of ATPD (in terms of mV depolarized from −80 mV) remained constant once it reached the maximum, indicative of an all-or-none response (Fig. 4(Ac)).

Besides the 83 % of neurons that responded with ATPD to at least one of the injection steps, 13 % (10/75) neurons showed obvious depolarizing response that extended briefly beyond the end of the injection pulse but did not reach a plateau (Fig. 4(Ad, D)). In line with the above classification, we designated these responses as BTD at CC-80s. Different from the

CC-45 and CC-70 protocols, the maximal depolarization amplitudes of individual neurons were not segregated between BTD and ATPD at CC-80s (Fig. 4(C)). The majority of the neurons that had ATPD also displayed BTD in steps either before or after those that showed ATPD (for example, see Fig. 4(Ac)), indicating that BTD represents partial activation while ATPD represents full activation of ion channels that underlie mGluR agonist-evoked depolarization. Finally, the remaining three WT LS neurons (4 %, 3/75) failed to respond to DHPG with either ATPD or BTD under the CC-80s protocol (Fig. 4(D)). Importantly, neither ATPD nor BTD was evoked in LS neurons from TRPC4$^{-/-}$ mice (Fig. 4(B)). Quantification of area under the trace revealed that the overall depolarization in response to current injection and DHPG ejection in LS neurons from TRPC4$^{-/-}$ mice was not different from that of WT neurons with current injection and aCSF ejection; however, it was significantly lower than that of WT neurons showing ATPD or BTD in response to current injection and DHPG ejection (Fig. 4(E)). These results again confirm that both ATPD and BTD are dependent on the expression of TRPC4. Since the responses of ATPD and BTD at CC-80s in WT neurons are clearly distinguishable from that of TRPC4$^{-/-}$ LS neurons, results from this protocol were used for quantification in the following mechanistic studies.

Transformation between BTD and ATPD neurons under different recording conditions

Because the majority of LS neurons reported above were recorded using all three current clamp protocols, we were able to compare the responses of the same neuron to DHPG ejection under these different recording conditions. As indicated above, the percentage of WT LS neurons that displayed ATPD increased from about 46 % with CC-70 to 70 % with CC-45 (for both firing and non-firing cells), and 83 % with the CC-80s protocol. This indicates that some neurons showing BTD in CC-70 must have acquired ATPD under the other two protocols. To reveal the transformation between BTD and ATPD in individual LS neurons, we plotted the maximal depolarization elicited by DHPG ejection for each neuron under all three conditions (Fig. 5(A, B)). Interestingly, in all BTD neurons at CC-70, 65 % (26/40 tested) transformed to ATPD (ΔmV >20 mV) at CC-45 and 85 % (34/40 tested) became ATPD (ΔmV >30 mV) at CC-80s (Fig. 5(A, C)). Conversely, only a small percentage of the ATPD neurons at CC-70 transformed to BTD under CC-45 (15 %, 4/27 tested) and CC-80s (20 %, 7/35 tested) conditions (Fig. 5(B, C)). Thus, >50 % of cells that showed ATPD at CC-45 (26/49) and CC-80s (34/62) were from BTD neurons at CC-70 and these cells were indistinguishable from those that were originally ATPD neurons at CC-70 in terms of the maximal depolarization elicited by DHPG ejection at CC-45 and CC-80s (Fig. 5(D)). These results demonstrate that the BTD neurons at CC-70 were capable of generating ATPD just like the ATPD neurons at CC-70, but they required either more depolarized V_m or co-incident current injection, which activates voltage-gated Na^+ and Ca^{2+} channels. The positive correlations of ATPD amplitudes between CC-45 and CC-80s for individual BTD neurons at CC-70 (Fig. 5(E)) and among all three stimulation paradigms for individual ATPD neurons at CC-70 (Fig. 5(F)) suggest that the ion channel mechanism that underlies ATPD must be similar among all three stimulation paradigms and the BTD represents responses that fail to reach the threshold for plateau depolarization. Since ATPD is more likely to occur at CC-45 and CC-80s than at CC-70, other factors, in addition to activation of mGluRs, must be important for the induction of ATPD. Altogether, the above results revealed that BTD and ATPD are two interconvertible responses of LS neurons to

DHPG stimulation, which involve both group 1 mGluRs and TRPC4-cc and reflect different levels of TRPC4-cc activation.

Ionic current induced by ejection of DHPG onto LS neurons

A selected number of LS neurons were also studied by whole-cell voltage clamp recordings. Cells were voltage-clamped at −70 mV and DHPG (30 μM) was puffed towards the somata without or with a 200-ms voltage step to −10 mV coinciding with the beginning of the drug ejection. In the absence of the voltage step (VC-70), ejecting aCSF did not affect the basal current (Fig. 6(Aa)), but ejecting DHPG elicited two types of responses in WT LS neurons: a small long-lasting inward current (Fig. 6(Ab)) or a large but transient inward current (Fig. 6(Ac, d)). LS neurons from TRPC4$^{-/-}$ mice, however, only showed small and slowly developing inward currents in response to DHPG (Fig. 6(B)). The time to peak for the current in TRPC4$^{-/-}$ LS neurons (7.1±1.6 s, n =8) was about twice that of WT neurons that showed small long-lasting current (3.7±0.5 s, n =36, P =0.014 vs TRPC4$^{-/-}$). These results suggest that the major component of the inward current seen in the WT LS neurons, especially those that showed large transient current, was mediated by TRPC4-cc. However, DHPG also activated other channels, which gave rise to the small inward currents seen in TRPC4$^{-/-}$ LS neurons.

With the concurrent voltage step (−10 mV, 200 ms, with a 50-ms prepulse to −45 mV to inactivate voltage-gated Na^+ channels, VC-70s, Fig. 6(Ca)), DHPG ejection evoked a robust response in nearly all WT LS neurons (33/35 tested), which was seen as a large tail current upon returning to −70 mV (Fig. 6(Cb)). The response was not seen without DHPG ejection and was completely absent in TRPC4$^{-/-}$ LS neurons (Fig. 6(D)). No matter if the WT LS neurons had small or large currents under the VC-70 protocol, the maximal currents obtained from the neurons using the VC-70s protocol were similar (Fig. 6E). Compared to VC-70, the distribution of current amplitudes obtained using the VC-70s protocol was shifted markedly to the right (Fig. 6(F)). These results demonstrate a strong enhancing effect of the step depolarization on DHPG-evoked TRPC4-cc activation in LS neurons, probably through Ca^{2+} entry mediated by VGCCs (see later).

Correlation analyses between VC-70 and CC-70 revealed that BTD neurons at CC-70 only developed small long-lasting current at VC-70. By contrast, the large transient current only developed in a subset of neurons that had ATPD at CC-70 (Fig. 6(G), exponential fit). The rest of the ATPD neurons only showed small long-lasting inward current (Fig. 6(G), linear fit), implying that the voltage clamp at −70 mV is even more suboptimal for activation of TRPC4-cc than current clamp at −70 mV. A major difference between the VC-70 and CC-70 protocols is that the current clamp mode allowed membrane depolarization in response to TRP channel activation, which on top of the Ca^{2+} influx mediated by the TRP channels could trigger additional Ca^{2+} entry through VGCCs. However, the activation of VGCCs was dependent on whether the initial depolarization elicited by TRPC4-cc activation could reach the threshold for the generation of action potentials, i.e., that of voltage-gated Na^+ channels. The above results, thus, can be interpreted as that the BTD neurons at CC-70 never reached the threshold for VGCC activation and a subset of the ATPD neurons generated the plateau depolarization at CC-70 with the facilitation by VGCCs but could not

sustain a strong TRPC4-cc activity at VC-70 in the absence of VGCC activation. These neurons, therefore, only developed the small sustained currents at VC-70. The remaining neurons at VC-70 probably had a strong initial activity that supported sufficient Ca^{2+} entry through the activated TRPC4-cc to allow for a positive feedback loop to cause the large transient currents. Consistent with the above interpretation, the depolarizing step in the VC-70s protocol allowed for development of the large transient currents in all tested neurons (Fig. 6(G)).

The role of postsynaptic group I mGluRs in DHPG-evoked ATPD in LS neurons

Postsynaptic group I mGluRs, including mGluR1 and mGluR5, are the most likely targets of DHPG for coupling to TRPC4-cc activation to induce ATPD in LS neurons. To confirm the involvement of mGluR1 and mGluR5, we included 30 μM YM298198, a mGluR1-specific antagonist, and 10 μM MPEP, a mGluR5-specific antagonist, in the ejection solution with DHPG. These drugs nearly completely abolished ATPD (Fig. 7(A, B)).

The above experiments had used 30 μM DHPG because it successfully induced ATPD in the majority of LS neurons. To determine the concentration dependence, we also tested a range of DHPG concentrations from 1 to 200 μM using the CC-80s protocol. Ejecting 1 μM DHPG failed to evoke either ATPD or BTD in WT LS neurons. Ejecting 5 μM DHPG only evoked BTD in 40 % of tested LS neurons. At 10 μM or higher concentrations, DHPG evoked both ATPD and BTD in LS neurons and the BTD/ ATPD ratio stabilized between 30 and 200 μM DHPG (Fig. 7(C)). Calculating the area under the trace for all evoked responses using the CC-80s protocol revealed an EC_{50} of 9.0 μM for DHPG-evoked responses in WT LS neurons (Fig. 7(D)).

Recordings of neurons from $TRPC4^{-/-}$ mice provided direct evidence that DHPG-evoked ATPD in LS neurons was dependent on TRPC4. Consistent with this conclusion, inclusion of the nonselective cation channel blocker, SKF96365, and the recently described TRPC4/C5 blocker, ML204 [17], in the injection solution with DHPG, significantly supressed the induction of ATPD (data not shown).

Besides activating the targeted LS neurons, DHPG ejection might also excite adjacent cells to release undefined neuro-transmitters that promoted ATPD in the recorded neurons. To test whether activity-dependent release of extrinsic signals from surrounding neurons contributes to the DHPG effects, we pretreated the brain slice with 1 μM TTX in aCSF and also included 1 μM TTX in the ejection solution together with 30 μM DHPG. As shown in Fig. 8(A) and summarized in Fig. 8(G), TTX successfully blocked the generation of action potentials, but did not significantly impair the induction of ATPD by DHPG. Altogether, these results suggest that postsynaptic group I mGluRs are responsible for triggering TRPC4-cc activation in LS neurons in response to DHPG, and TTX-sensitive Na^+ channels are not absolutely required for TRPC4-cc-mediated ATPD.

Contributions of Na^+ and Ca^{2+} influx and intracellular Ca^{2+} dynamics to the induction of ATPD

The finding that current injection facilitated the development of ATPD in response to stimulation of mGluRs suggested that either the more depolarized membrane potential or the

activation of voltage-gated Na^+ and/or Ca^{2+} channels enhanced the activation of TRPC4-cc. Previous studies have demonstrated the importance of intracellular Ca^{2+} on the activation of TRPC4 and TRPC5 [2, 13, 31] as well as the contribution of Ca^{2+} influx through VGCCs on TRPC5-like currents in neurons [38, 39]. However, it was not known to what extent the Na^+ influx, through either voltage-gated Na^+ channels or TRPC4-cc, contributed to the activation of TRPC4-cc in neurons. We therefore examined the requirement on Na^+ and Ca^{2+} influx of ATPD induction by DHPG in LS neurons. First, we excluded the requirement of TTX-sensitive Na^+ channels by showing that ATPD was successfully induced by DHPG in the presence of 1 μM TTX under all three stimulation paradigms (Fig. 8(A, G)). We then recorded LS neurons in a choline-Cl aCSF (NaCl was substituted with choline-Cl, with the Na^+ concentration reduced to ∼27 mM) and showed that only BTD was successfully evoked (Fig. 8(B)). Therefore, Na^+ influx via the TRPC4-cc is critical for the induction of ATPD, meaning that without sufficient Na^+ influx, Ca^{2+} influx through TRPC4-cc, and even with participation of VGCCs (CC-80s protocol), is unable to induce ATPD. Next, we recorded LS neurons in a nominally Ca^{2+}-free aCSF. Perfusion of the brain slice with the nominally Ca^{2+}-free aCSF caused large fluctuations of the membrane potential and firing of LS neurons held at −70 mV (data not shown). To remove the Na^+ spikes, we included 1 μM TTX in the nominally Ca^{2+}-free aCSF. Notably, when using the CC-70 and CC-45 protocols, ejecting DHPG under this condition evoked membrane depolarization that shared similar kinetic properties as BTD but with a higher degree of depolarization than BTD (Fig. 8(C)). However, no ATPD was induced with the use of CC-80s protocol in the nominally Ca^{2+}-free aCSF (Fig. 8(C, G)). Thus, the enhanced depolarization at CC-70 and CC-45 could represent a disinhibition during BTD of TRPC4-cc at the reduced extracellular Ca^{2+} level, which occurs under conditions when TRPC4 is weakly activated but not when it is strongly activated (D.P.T and M.X.Z, unpublished observation). The induction of ATPD is still dependent on Ca^{2+} influx.

To test the involvement of VGCCs, we included an L-type VGCC blocker, nifedipine (30 μM), in the ejection solution and detected a significant inhibition of DHPG-induced ATPD in LS neurons (Fig. 8(D, G)). The inhibition by nifedipine was highly variable, which could be attributed to differences in the subtypes of VGCCs present in individual LS neurons.

To test the role of intracellular Ca^{2+} on the induction of ATPD, we used 10 mM BAPTA, a fast Ca^{2+} chelator, instead of 0.05 mM EGTA to buffer Ca^{2+} in the internal solution. In the first set of experiments, the pipette solution contained 10 mM BAPTA with no added Ca^{2+} (free $[Ca^{2+}]$ <10 nM). Interestingly, most tested LS neurons displayed burst firing at CC-45, but no ATPD was induced by ejecting DHPG under all recording conditions (Fig. 8(E)). In the second set of experiments, the pipette solution contained 10 mM BAPTA and 7.24 mM $CaCl_2$ (free $[Ca^{2+}]$ ∼600 nM) in order to provide an elevated intracellular $[Ca^{2+}]$ but not allow it to change in response to stimuli. With this pipette solution, DHPG ejection also failed to induce ATPD under all three protocols (Fig. 8(F)). Quantifications of ATPD under the CC-80s conditions for all manipulations described above revealed that the induction of ATPD was strongly compromised by the removal of Na^+ or Ca^{2+} from the extracellular solution or inhibition of Ca^{2+} dynamics from the cytoplasmic side (Fig. 8(G)). Taken together, our data demonstrate that influx of both Na^+ and Ca^{2+}, along with dynamic

changes in intracellular Ca^{2+} (not simply an elevated intracellular Ca^{2+} level per se), are necessary for the induction of ATPD by the mGluR agonist in LS neurons.

Temporal relationship between mGluR stimulation and VGCC activation for strong activation of TRPC4-cc

The above conclusions were confirmed in voltage clamp experiments using the VC-70s protocol (data not shown). Although the Na^+ and Ca^{2+} requirement for the "inward aftercurrent" in rat lateral septal neurons in response to depolarization steps during the whole-chamber perfusion of 1S, 3R-ACPD has been demonstrated previously [28], we showed that, supporting the conclusion from the current clamp experiments, intracellular Ca^{2+} dynamics were critical for the development of the large TRPC4-cc current. With intracellular dialysis of 10 mM BAPTA to prevent Ca^{2+} fluctuations, the VC-70s protocol failed to elite any discernible TRPC4-cc-like current no matter if the free $[Ca^{2+}]$ was maintained at a very low level (<10 nM) or at an elevated level (600 nM) (Fig. 9(A, B)).

Because both mGluR stimulation and intracellular Ca^{2+} dynamics are required for the strong activation of TRPC4-cc, we explored the temporal relationship between these two processes using the VC-70s protocol, but with varying time intervals (Δt) between DHPG ejection and the −10 mV depolarization step, as well as varying step durations. We found that ejecting DHPG (always at 30 μM for 30 ms) at the beginning of the 200-ms step to −10 mV gave the most robust response (Fig. 9(C–E), traces for Δt =0). When DHPG was ejected at the end of the 200-ms step, no TRPC4-cc current was detected (Fig. 9(D, E), traces for Δt =200). Ejecting DHPG 50 ms before the start of the 200-ms step to −10 mV did not compromise the development of the TRPC4-cc current (Fig. 9(D, E), Δt =−50 trace), but further extending the interval to −150 and −300 ms decreased the current, with the −300-ms interval becoming ineffective in inducing the TRPC4-cc current (Fig. 9(D, E), traces for Δt =−150, Δt =−300). The step duration at −10 mV also affected the current. While shorter steps (50 and 100 ms) were less effective at inducing the large TRPC4-cc current than the 200-ms step, a longer step (300 ms) also yielded smaller current than the 200-ms step (Fig. 9(F)), probably because the extended 100 ms depolarization masked a large portion of the TRPC4-cc current. These results indicate that not only is the timing between mGluR stimulation and VGCC activation critical but also the duration of VGCC activation is important for the induction of the strong TRPC4-cc current.

Discussion

The foregoing data demonstrate two distinct effects of TRPC4-cc activation in LS neurons, dependent on the relative degree of channel activity. The BTD represents weak whereas ATPD reflects strong activation of TRPC4-cc by the mGluR agonist. Studies in heterologous systems have revealed the intricate dependence of TRPC4 and C5 activation on intracellular Ca^{2+}, in addition to PLC stimulation [21, 31]. The Ca^{2+} signal strongly enhances TRPC4/C5 activation, resulting in further elevation of intracellular Ca^{2+} by Ca^{2+} influx through the activated TRPC channels. This forms a positive feedback loop reminiscent of activation of voltage-gated Na^+ channels by depolarization. Also similar to the Na^+ channels, TRPC4/ C5 channels undergo inactivation during continued stimulation,

probably because of inhibition by high intracellular [Ca^{2+}] [21] or self-limiting regulation by PLC-mediated breakdown of PIP_2 [15, 16]. However, moderate activation of TRPC4 is possible at the resting intracellular [Ca^{2+}] (∼100 nM, buffered by 10 mM BAPTA) and in the absence of extracellular Ca^{2+} [22], providing a Ca^{2+}-independent mode of activation, which could underlie BTD in LS neurons.

The development of ATPD, hence, may require raising the intracellular [Ca^{2+}] to above the threshold needed to generate the positive feedback loop to potentiate TRPC4 currents. The threshold [Ca^{2+}] for such an effect is unknown, but the Ca^{2+} sources include Ca^{2+} release from internal stores and Ca^{2+} influx from extracellular space. The internal Ca^{2+} store release, which is a necessary component of the $G_{q/11}$-PLC pathway activated by the group 1 mGluRs, appears to be insufficient to trigger ATPD, as no ATPD was detected in the nominally Ca^{2+}-free aCSF. Ca^{2+} influx can be mediated by the activated TRPC4-cc and/or VGCCs. In the current clamp mode, it is hard to separate these two pathways, since the initial influx may be mediated by the moderately activated TRPC4-cc, but once the depolarization reaches the firing threshold, VGCCs should bring in a bolus of Ca^{2+}, causing a strong potentiation of TRPC4-cc. This explains why current injection greatly facilitated ATPD induction. Under normal conditions, the threshold of voltage-gated Na^+ channels should be an important factor irrespective of whether it was reached due to TRPC4-cc mediated depolarization or current injection. This threshold, however, mainly serves to trigger subsequent activation of VGCCs, through which the Ca^{2+} influx reaches the Ca^{2+} threshold critical for ATPD induction. Therefore, the Na^+ channels are not absolutely required as ATPD was inducible in the presence of TTX.

Our data also suggest that just having action potentials coincident with DHPG application may not be sufficient for ATPD induction, as BTD was detected in some firing neurons at CC-45 and in some injection steps at CC-80s when action potential was elicited. Under voltage-clamped conditions, a step depolarization to −10 mV for 200 ms appeared to be optimal for inducing the strong TRPC4-cc current, suggesting that extended VGCC activation may be necessary for reaching the Ca^{2+} threshold of ATPD induction. However, we do not exclude the possibility that TRPC4-cc activation could also be enhanced by the depolarization-induced change of mGluRs to a high affinity ligand-binding state [11]. Indeed, the occurrence of ATPD depended on the concentration of DHPG.

The requirement for VGCCs may also be optional given that large transient currents were induced by DHPG in some LS neurons held at −70 mV (VC-70 protocol). This can be interpreted in two ways: one would be the uneven membrane voltages across the cells because of the space clamp issue such that VGCC activities still existed in some regions of the responding cells; the second would be that the TRPC4-cc densities were high enough in the responding cells so that the Ca^{2+}-independent activation, equivalent to the condition of BTD, could bring in enough Ca^{2+} through the activated TRPC4-cc to reach the Ca^{2+} threshold for positive feedback potentiation. The latter interpretation is consistent with the fact that large inward currents are commonly detected in heterologous cells that overexpress TRPC4 but without any VGCC activity, indicating that TRPC4 expression alone can support strong activation, especially when expressed at high levels. Nonetheless, VGCC activation strongly facilitated this Ca^{2+}-dependent mode of TRPC4-cc activation, as seen with a

depolarizing step at VC-70s. Intriguingly, TRPC4-cc activation was still facilitated by the depolarization step initiated 150 ms after the application of DHPG (or 120 ms after the end of the 30 ms ejection) but not that initiated 200 ms before mGluR stimulation, suggesting an important temporal relationship between mGluR stimulation and VGCC activation (or Ca^{2+} signal). It appears that the Ca^{2+} signal needs to either coincide with or arise shortly after the mGluR stimulation, at least under voltage-clamped conditions.

We found a complete absence of ATPD in TRPC4$^{-/-}$ LS neurons in response to DHPG, suggesting that ATPD is absolutely dependent on TRPC4-cc. The BTD is not as clean and probably contains responses from non-TRPC4 channels. However, given the much slower time-to-peak response found in TRPC4$^{-/-}$ neurons than WT BTD neurons, the initial phase of BTD (at CC-70 and CC-45) should reflect primarily the activity of TRPC4-cc. This is consistent with the finding that no BTD-like response was detected in TRPC4$^{-/-}$ LS neurons using CC-80s, which was designed to record shorter term responses than the other two protocols. Importantly, BTD and ATPD are interconvertible in individual LS neurons. The switch from BTD to ATPD was clearly facilitated by membrane depolarization, e.g., from the holding potential of −70 to −45 mV or by positive current injection with the holding at −80 mV. As discussed above, this facilitation was most likely mediated by the opening of VGCCs, which helps reach the Ca^{2+} threshold for positive feedback potentiation of TRPC4 function, a notion supported by the finding that chelating intracellular Ca^{2+} with BAPTA completely abolished ATPD induction. Interestingly, maintaining a steady-state high intracellular free [Ca^{2+}] (∼600 nM) but preventing it from fluctuating with 10 mM BAPTA also did not allow ATPD, suggesting the importance of dynamic changes of cytosolic Ca^{2+} for ATPD induction. On the other hand, the reason for the relatively rare switch from ATPD at CC-70 to BTD at CC-45 or CC-80s is unclear. Possibilities include inhibition of TRPC4-cc by higher [Ca^{2+}] and channel desensitization.

It has been suggested that TRPC4, and TRPC5, together with TRPC1, underlie afterdepolarization or plateau potentials following GPCR stimulation in neurons. In order to generate plateau depolarization, concurrent application of either high-frequency electrical stimulation to the afferent inputs or current injection to the target neuron is typically implemented in addition to stimulation by a GPCR agonist [6–8, 18, 36, 39]. Occasionally, plateau depolarization has been induced with an mGluR agonist alone, delivered via whole-chamber perfusion [23]. Here, we demonstrate that a brief pressure ejection of DHPG alone onto somata of single LS neurons can induce burst firing and plateau depolarization, albeit at a lower efficiency than with current injection. Intriguingly, ∼3 % (5/ 162) of LS neurons spontaneously displayed similar burst firing and plateau depolarization under our whole-cell conditions. Previous study using intracellular recordings revealed about 15 % of “burster” rat dorsolateral septal neurons, which exhibited burst firing at membrane potentials from −50 to −60 mV [10, 14]. The lower frequency in our observation may be due to the greater disturbance of the cytoplasm in the whole cell mode than in the sharp electrode recording configuration and/or the relatively short time period (∼7 s) of recording of spontaneous activities for each neuron. Notably, bursting LS neurons often display rhythmicity in the theta range, i.e., 3–12 Hz, with the burst appearing at the peak of each cycle [10]. Therefore, burst firing may account for the generation of theta rhythm, one of the important functions of the septal nuclei.

The impact of BTD and ATPD on LS neuron firing is worth noting. While BTD increased firing frequency, ATPD caused, typically, immediate bursting followed by a pause of firing that lasted for variable durations. This bimodal modulation of LS neuron excitability by a brief stimulation of group 1 mGluRs was evident in both whole-cell and loose-patch configurations, demonstrating that the results obtained from whole-cell recordings faithfully represented natural responses of these neurons to TRPC4-cc activation. Thus, the group 1 mGluR-mediated TRPC4-cc activation can either be purely excitatory or both excitatory and inhibitory with complex response patterns depending on the relative degree of channel activity. Like other nonselective cation channels, TRPC channel activations are frequently linked to excitation. The demonstration that TRPC4-cc activation can also stop LS neurons from firing, likely by strongly depolarizing the membrane to inactivate voltage-gated Na^+ channels, indicates that TRPC channels can respond to metabotropic signaling with complex outcomes on neuronal excitability, including inhibition. This dual regulation implicates a strong impact of the GPCR-TRPC pathway in neuronal functions.

The lateral septum is traditionally thought to be a simple relay center in the CNS. Recent studies suggest that it actively processes as well as relays information [10, 32]. LS neurons receive synaptic inputs and send out processed information to broad brain areas [10, 29, 30, 32]. Excitatory synaptic inputs from the prefrontal cortex and hippocampus may activate TRPC4-cc through mGluRs and other GPCRs expressed on LS neurons. Then, depending on the degree of TRPC4-cc activation, these inputs may either excite or inhibit LS neurons, conveying information for important brain functions such as motivation, anxiety, and depression, which are known to be modulated by the lateral septum [32].

Acknowledgments

We thank Dr. E. T. Walters for critical comments on the manuscripts, Dr. X. Hong for ML204 and members of the Zhu lab for helpful discussion about the project. This work was supported in part by US National Institutes of Health grants DK081654 and GM092759.

Abbreviations

ATPD	Above-threshold-plateau-depolarization
BTD	Below-threshold-depolarization
CC-45	Current clamp with the initial potential of −45 mV
CC-70	Current clamp with the initial potential of −70 mV
CC-80s	Current clamp at −80 mV with current pulse injections
DHPG	(*S*)-3,5-Dihydroxyphenylglycine
GPCRs	G protein-coupled receptors
LS	Lateral septal
mGluRs	Metabotropic glutamate receptors
PLC	Phospholipase C
TRPC	Canonical transient receptor potential

TRPC4-cc	TRPC4-containing channels
VC-70	Voltage clamp at −70 mV
VC-70s	Voltage clamp at −70 mV with a pre-voltage step to −10 mV
VGCCs	Voltage-gated Ca^{2+} channels
WT	Wild type

References

1. Birnbaumer L. The TRPC class of ion channels: a critical review of their roles in slow, sustained increases in intracellular Ca^{2+} concentrations. Annu Rev Pharmacol Toxicol. 2009; 49:395–426. [PubMed: 19281310]
2. Blair NT, Kaczmarek JS, Clapham DE. Intracellular calcium strongly potentiates agonist-activated TRPC5 channels. J Gen Physiol. 2009; 133:525–546. [PubMed: 19398778]
3. Cavalie A. Ionic channels formed by TRPC4. Handb Exp Pharmacol. 2007; 179:93–108. [PubMed: 17217052]
4. Chung YH, Sun Ahn H, Kim D, Hoon Shin D, Su Kim S, Yong Kim K, Bok Lee W, Ik Cha C. Immunohistochemical study on the distribution of TRPC channels in the rat hippocampus. Brain Res. 2006; 1085:132–137. [PubMed: 16580647]
5. Clapham DE, Runnels LW, Strubing C. The TRP ion channel family. Nat Rev Neurosci. 2001; 2:387–396. [PubMed: 11389472]
6. El-Hassar L, Hagenston AM, D'Angelo LB, Yeckel MF. Metabotropic glutamate receptors regulate hippocampal CA1 pyramidal neuron excitability via Ca^{2+} wave-dependent activation of SK and TRPC channels. J Physiol Lond. 2011; 589:3211–3229. [PubMed: 21576272]
7. Faber E, Sedlak P, Vidovic M, Sah P. Synaptic activation of transient receptor potential channels by metabotropic glutamate receptors in the lateral amygdala. Neuroscience. 2006; 137:781–794. [PubMed: 16289832]
8. Fowler M, Sidiropoulou K, Ozkan E, Phillips C, Cooper D. Corticolimbic expression of TRPC4 and TRPC5 channels in the rodent brain. PLoS ONE. 2007; 2:e573. [PubMed: 17593972]
9. Freichel M, Suh SH, Pfeifer A, Schweig U, Trost C, Weissgerber P, Biel M, Philipp S, Freise D, Droogmans G, Hofmann F, Flockerzi V, Nilius B. Lack of an endothelial store-operated Ca^{2+} current impairs agonist-dependent vasorelaxation in $TRP4^{-/-}$ mice. Nat Cell Biol. 2001; 3:121–127. [PubMed: 11175743]
10. Gallagher JP, Zheng F, Hasuo H, Shinnick-Gallagher P. Activities of neurons within the rat dorsolateral septal nucleus (DLSN). Prog Neurobiol. 1995; 45:373–395. [PubMed: 7617889]
11. Gerber U, Gee C, Benquet P. Metabotropic glutamate receptors: intracellular signaling pathways. Curr Opin Pharmacol. 2007; 7:56–61. [PubMed: 17055336]
12. Goel M, Sinkins W, Schilling W. Selective association of TRPC channel subunits in rat brain synaptosomes. J Biol Chem. 2002; 277:48303–48310. [PubMed: 12377790]
13. Gross SA, Guzmán GA, Wissenbach U, Philipp SE, Zhu MX, Bruns D, Cavalié A. TRPC5 is a Ca^{2+}-activated channel functionally coupled to Ca^{2+}-selective ion channels. J Biol Chem. 2009; 284:34423–34432. [PubMed: 19815560]
14. Hasuo H, Phelan KD, Twery MJ, Gallagher JP. A calcium-dependent slow afterdepolarization recorded in rat dorsolateral septal nucleus neurons in vitro. J Neurophysiol. 1990; 64:1838–1846. [PubMed: 2074467]
15. Imai Y, Itsuki K, Okamura Y, Inoue R, Mori MX. A self-limiting regulation of vasoconstrictor-activated TRPC3/C6/C7 channels coupled to $PI(4,5)P_2$-diacylglycerol signalling. J Physiol Lond. 2012; 590:1101–1119. [PubMed: 22183723]
16. Kim H, Jeon JP, Hong C, Kim J, Myeong J, Jeon JH, So I. An essential role of PI(4,5)P(2) for maintaining the activity of the transient receptor potential canonical (TRPC)4beta. Pflugers Arch. 2013

17. Miller M, Shi J, Zhu Y, Kustov M, Tian JB, Stevens A, Wu M, Xu J, Long S, Yang P, Zholos AV, Salovich JM, Weaver CD, Hopkins CR, Lindsley CW, McManus O, Li M, Zhu MX. Identification of ML204, a novel potent antagonist that selectively modulates native TRPC4/C5 ion channels. J Biol Chem. 2011; 286:33436–33446. [PubMed: 21795696]
18. Moore SJ, Cooper DC, Spruston N. Plasticity of burst firing induced by synergistic activation of metabotropic glutamate and acetylcholine receptors. Neuron. 2009; 61:287–300. [PubMed: 19186170]
19. Mori Y, Takada N, Okada T, Wakamori M, Imoto K, Wanifuchi H, Oka H, Oba A, Ikenaka K, Kurosaki T. Differential distribution of TRP Ca^{2+} channel isoforms in mouse brain. Neuroreport. 1998; 9:507–515. [PubMed: 9512398]
20. Munsch T, Freichel M, Flockerzi V, Pape H-C. Contribution of transient receptor potential channels to the control of GABA release from dendrites. Proc Natl Acad Sci U S A. 2003; 100:16065–16070. [PubMed: 14668438]
21. Ordaz B, Tang J, Xiao R, Salgado A, Sampieri A, Zhu MX, Vaca L. Calmodulin and calcium interplay in the modulation of TRPC5 channel activity. Identification of a novel C-terminal domain for calcium/calmodulin-mediated facilitation. J Biol Chem. 2005; 280:30788–30796. [PubMed: 15987684]
22. Otsuguro K-I, Tang J, Tang Y, Xiao R, Freichel M, Tsvilovskyy V, Ito S, Flockerzi V, Zhu MX, Zholos AV. Isoform-specific inhibition of TRPC4 channel by phosphatidylinositol 4,5-bisphosphate. J Biol Chem. 2008; 283:10026–10036. [PubMed: 18230622]
23. Phelan K, Mock M, Kretz O, Shwe U, Kozhemyakin M, Greenfield L, Dietrich A, Birnbaumer L, Freichel M, Flockerzi V, Zheng F. Heteromeric canonical transient receptor potential 1 and 4 channels play a critical role in epileptiform burst firing and seizure-induced neurodegeneration. Mol Pharmacol. 2012; 81:384–392. [PubMed: 22144671]
24. Phelan K, Shwe U, Abramowitz J, Wu H, Rhee S, Howell M, Gottschall P, Freichel M, Flockerzi V, Birnbaumer L, Zheng F. Canonical transient receptor channel 5 (TRPC5) and TRPC1/4 contribute to seizure and excitotoxicity by distinct cellular mechanisms. Mol Pharmacol. 2013; 83:429–438. [PubMed: 23188715]
25. Plant TD, Schaefer M. TRPC4 and TRPC5: receptor-operated Ca^{2+}-permeable nonselective cation channels. Cell Calcium. 2003; 33:441–450. [PubMed: 12765689]
26. Plant TD, Schaefer M. Receptor-operated cation channels formed by TRPC4 and TRPC5. Naunyn-Schmiedeberg's Arch Pharmacol. 2005; 371:266–276. [PubMed: 15902430]
27. Qiu J, Fang Y, Ronnekleiv OK, Kelly MJ. Leptin excites proopiomelanocortin neurons via activation of TRPC channels. J Neurosci. 2010; 30:1560–1565. [PubMed: 20107083]
28. Raggenbass M, Pierson P, Metzger D, Alberi S. Action of a metabotropic glutamate receptor agonist in rat lateral septum: induction of a sodium-dependent inward aftercurrent. Brain Res. 1997; 776:75–87. [PubMed: 9439798]
29. Risold P, Swanson L. Chemoarchitecture of the rat lateral septal nucleus. Brain Res Brain Res Rev. 1997; 24:91–113. [PubMed: 9385453]
30. Risold P, Swanson L. Connections of the rat lateral septal complex. Brain Res Brain Res Rev. 1997; 24:115–195. [PubMed: 9385454]
31. Schaefer M, Plant T, Obukhov A, Hofmann T, Gudermann T, Schultz G. Receptor-mediated regulation of the nonselective cation channels TRPC4 and TRPC5. J Biol Chem. 2000; 275:17517–17526. [PubMed: 10837492]
32. Sheehan T, Chambers R, Russell D. Regulation of affect by the lateral septum: implications for neuropsychiatry. Brain Res Brain Res Rev. 2004; 46:71–117. [PubMed: 15297155]
33. Sidiropoulou K, Lu F-M, Fowler MA, Xiao R, Phillips C, Ozkan ED, Zhu MX, White FJ, Cooper DC. Dopamine modulates an mGluR5-mediated depolarization underlying prefrontal persistent activity. Nat Neurosci. 2009; 12:190–199. [PubMed: 19169252]
34. Stroh O, Freichel M, Kretz O, Birnbaumer L, Hartmann J, Egger V. NMDA receptor-dependent synaptic activation of TRPC channels in olfactory bulb granule cells. J Neurosci. 2012; 32:5737–5746. [PubMed: 22539836]

35. Strubing C, Krapivinsky G, Krapivinsky L, Clapham DE. Formation of novel TRPC channels by complex subunit interactions in embryonic brain. J Biol Chem. 2003; 278:39014–39019. [PubMed: 12857742]

36. Tai C, Hines DJ, Choi HB, MacVicar BA. Plasma membrane insertion of TRPC5 channels contributes to the cholinergic plateau potential in hippocampal CA1 pyramidal neurons. Hippocampus. 2011; 21:958–967. [PubMed: 20865744]

37. Wu LJ, Sweet TB, Clapham DE. International Union of Basic and Clinical Pharmacology. LXXVI. Current progress in the mammalian TRP ion channel family. Pharmacol Rev. 2010; 62:381–404. [PubMed: 20716668]

38. Yan H-D, Villalobos C, Andrade R. TRPC channels mediate a muscarinic receptor-induced afterdepolarization in cerebral cortex. J Neurosci. 2009; 29:10038–10046. [PubMed: 19675237]

39. Zhang Z, Reboreda A, Alonso A, Barker PA, Séguéla P. TRPC channels underlie cholinergic plateau potentials and persistent activity in entorhinal cortex. Hippocampus. 2011; 21:386–397. [PubMed: 20082292]

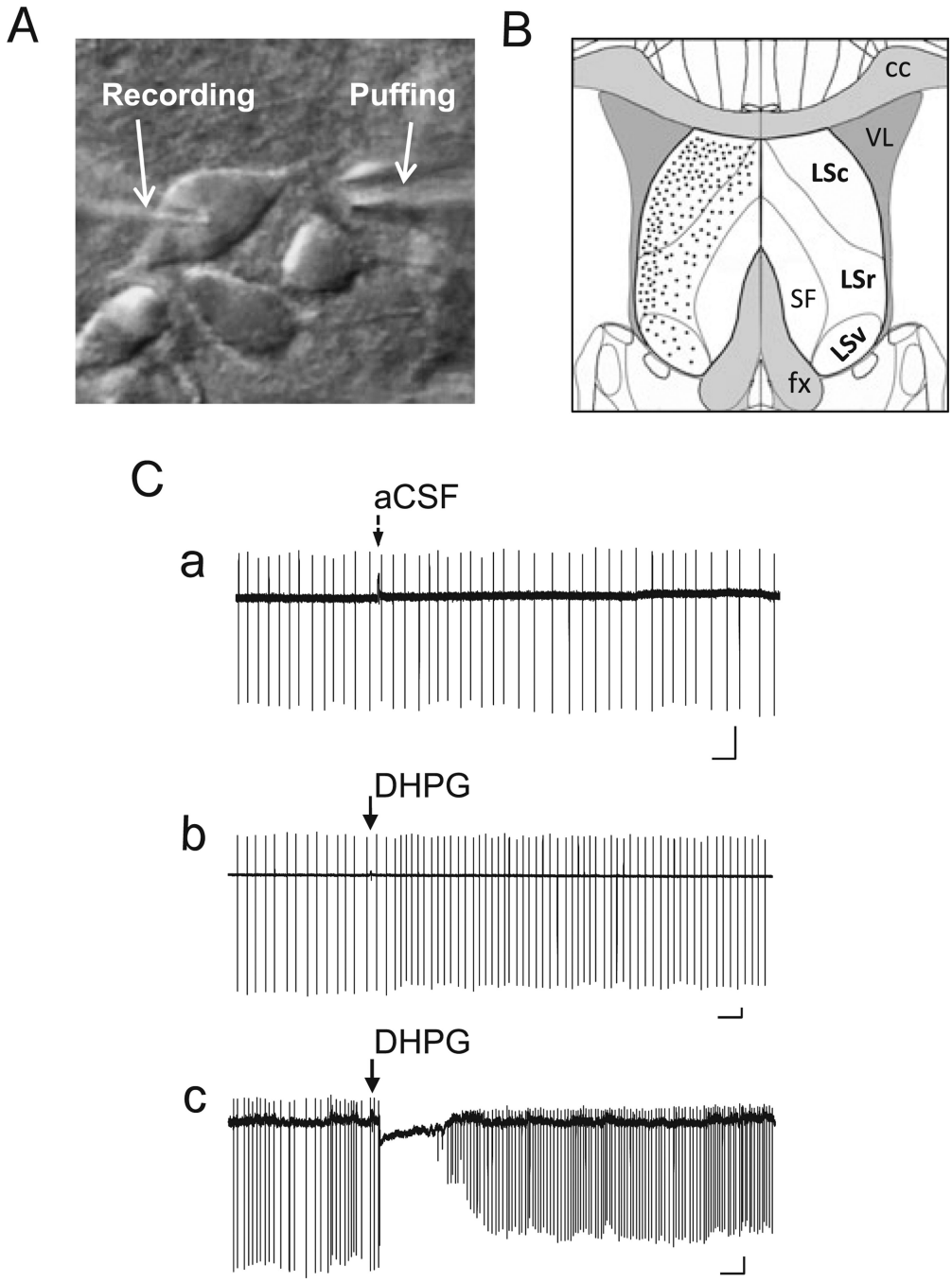

Fig. 1.

Pressure ejection of DHPG elicits two distinct response patterns of LS neuron firing in loose patch recordings. *A*, DIC image showing an LS neuron in brain slice held by a recording pipette and with an ejection electrode aimed at the dendrites near the soma. *B*, Diagram of coronal section of brain slice depicting the location and subdivisions of mouse lateral septal nucleus (*LSc*, *LSr*, and *LSv*). *Black dots* indicate the relative distribution of the LS neurons that were randomly picked for loose patch and whole-cell patch-clamp recordings in the current study. *C*, DHPG-evoked changes in firing patterns of LS neurons under loose-patch

recordings. Loose patches were made using recording pipette filled with aCSF. Representative traces showing changes of firing activity elicited by ejecting aCSF (*a*) or 30 μM DHPG (*b*, *c*; 5–20 psi, 30 ms) onto wild-type (WT) LS neurons. Note aCSF ejection did not interfere with LS firing (*Ca*), but DHPG ejection onto LS neurons elicited either an increase in firing rate (*Cb*) or a momentary pause of firing followed by an increase in firing rate (*Cc*). *Arrows* indicate the time of ejection of aCSF or DHPG. *Scale bars*: 0.5 s, 50 pA

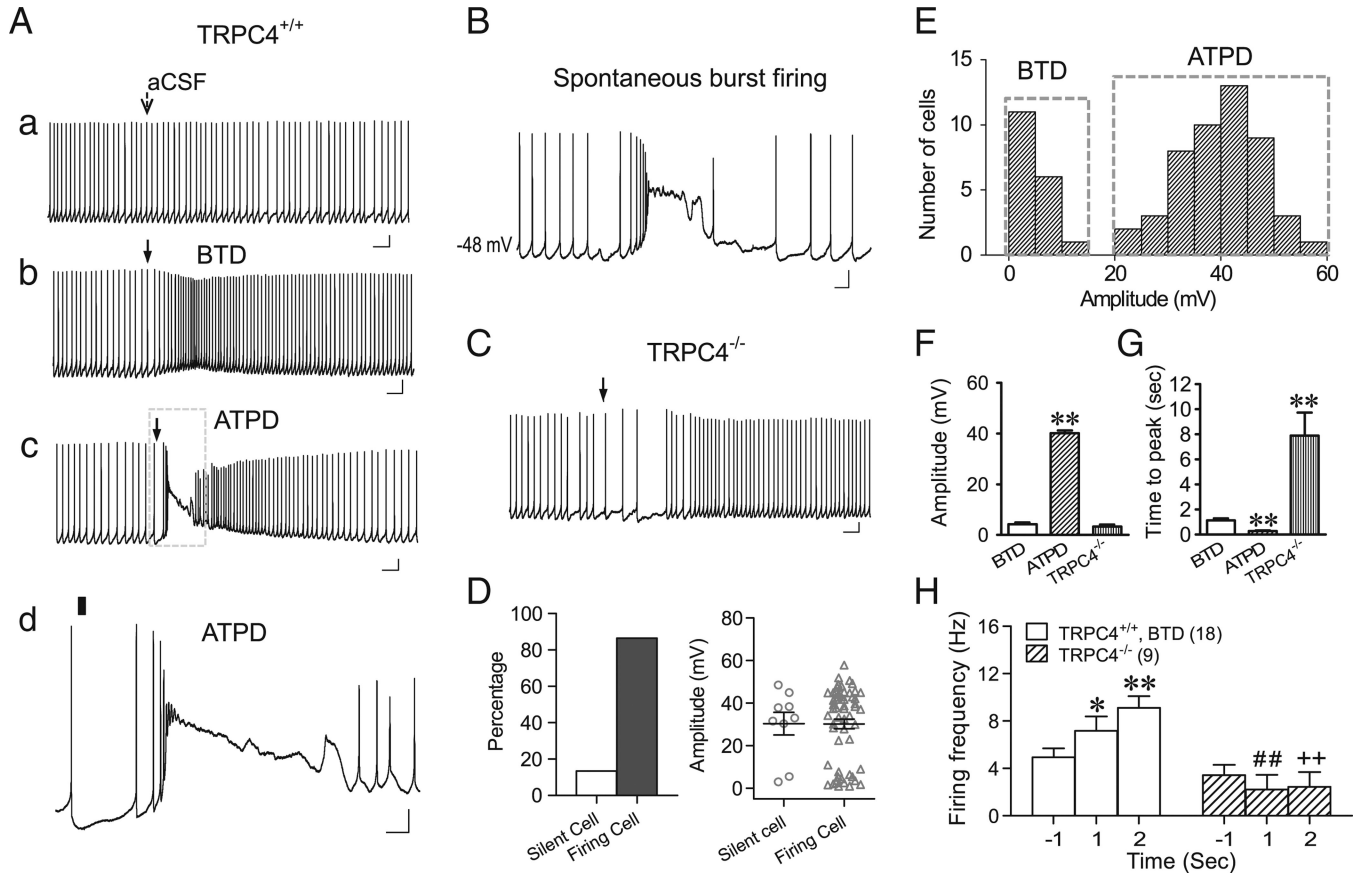

Fig. 2.

Pressure ejection of DHPG elicits below-threshold-depolarization (*BTD*) and above-threshold-plateau depolarization (*ATPD*) as well as the corresponding changes in membrane excitability of LS neurons in whole-cell recordings. *A*, Representative traces showing changes in membrane potential and firing activity elicited by ejecting aCSF (*a*) or 30 μM DHPG (*b–d*) onto WT (TRPC4$^{+/+}$) LS neurons held at −45 mV (CC-45). *Arrows* (*a–c*) indicate the time of ejection (5–20 psi, 30 ms). *d*, the boxed area of *c* in an expanded time scale with the ejection period indicated by the *black bar*. Note aCSF ejection did not change the resting membrane potential or interfere with LS firing (*a*), but DHPG ejection onto LS neurons elicited either BTD and the accompanied increase in firing rate (*b*) or ATPD, comprising an initial burst and then an extended plateau depolarization, and the accompanied burst firing followed by a momentary pause of firing during the plateau depolarization (*c* and *d* A T P D). *Scale bars*: 0.5 s, 10 mV (*a–c*); 100 ms, 10 mV (*d*). *B*, Example trace of spontaneous burst firing of an LS neuron during whole cell current clamp recording (without current injection). *Scale bars*: 100 ms, 10 mV. *C*, Similar to *Ab*, but showing that DHPG ejection onto the TRPC4$^{-/-}$ LS neuron elicited an initial decrease, followed by an increase in firing rate. *D*, *Left*, proportions of silent and firing TRPC4$^{+/+}$ LS neurons held at −45 mV. *Right*, scattered distributions and mean±SEM values of DHPG-evoked membrane depolarization of silent (*n* =9) and firing LS neurons (*n* =58). *E*, Distribution of peak depolarization amplitude evoked by DHPG ejection at CC-45 for TRPC4$^{+/+}$ neurons. Note the bimodal segregation of BTD and ATPD. *F*, *G*, Average (mean

±SEM) peak depolarization amplitudes (*F*) and time-to-peak values (G) of BTD (*n* =18) and ATPD (*n* =49) for TRPC4$^{+/+}$ and all TRPC4$^{-/-}$ LS neurons (*n*=9). ***P* <0.01, compared to BTD. *H*, Average firing frequency 1 s before and 1 and 2 s after DHPG ejection onto BTD TRPC4$^{+/+}$ and all TRPC4$^{-/-}$ LS neurons. **P*<0.05, ***P* <0.01, compared to BTD at −1 s; $^{\#\#,++}P$ <0.01, compared to BTD at 1 and 2 s, respectively

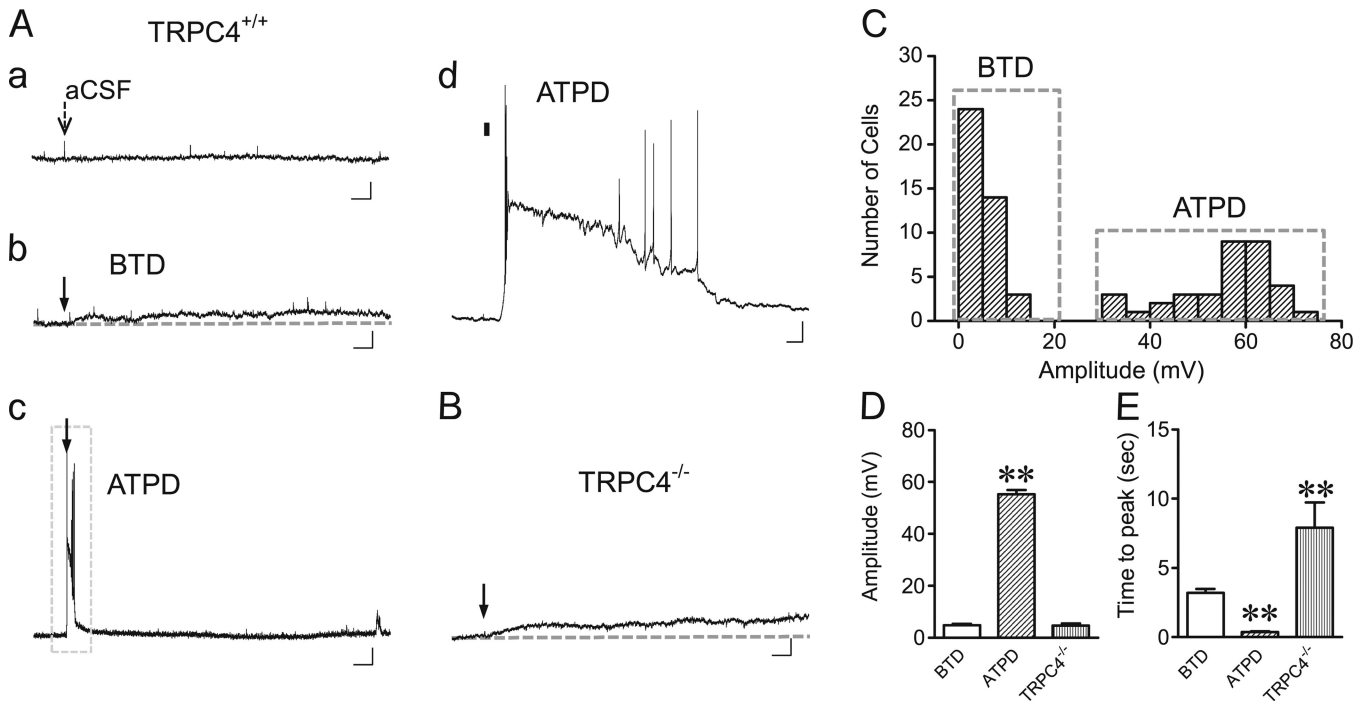

Fig. 3.

DHPG-evoked BTD and ATPD in LS neurons current clamped at −70 mV. *A*, Representative traces showing membrane potential changes elicited by ejecting aCSF (*a*) or 30 μM DHPG (*b*–*d*) onto WT (TRPC4$^{+/+}$) LS neurons held at −70 mV (CC-70). *Arrows* (*a*–*c*) indicate the time of ejection (5–20 psi, 30 ms). *d* The boxed area of *c* in an expanded time scale with the ejection period indicated by the *black bar*. Note ATPD also comprises an initial burst firing, followed by an extended plateau depolarization. Scale bars, 3 s, 10 mV (*a*–*c*); 100 ms, 10 mV (*d*). *B*, Similar to *Ab*, but for an LS neuron from TRPC4$^{-/-}$ mouse stimulated by DHPG ejection. *C*, Distribution of peak depolarization amplitudes evoked by DHPG ejection in TRPC4$^{+/+}$ LS neurons. Note the bimodal segregation of BTD and ATPD amplitudes. *D*, *E*, Average (mean±SEM) peak depolarization amplitudes (*D*) and time-to-peak values (*E*) of BTD (*n* =41) and ATPD (*n* =35) for TRPC4$^{+/+}$ neurons and all TRPC4$^{-/-}$ neurons (*n*=9). **P<0.01, compared to BTD

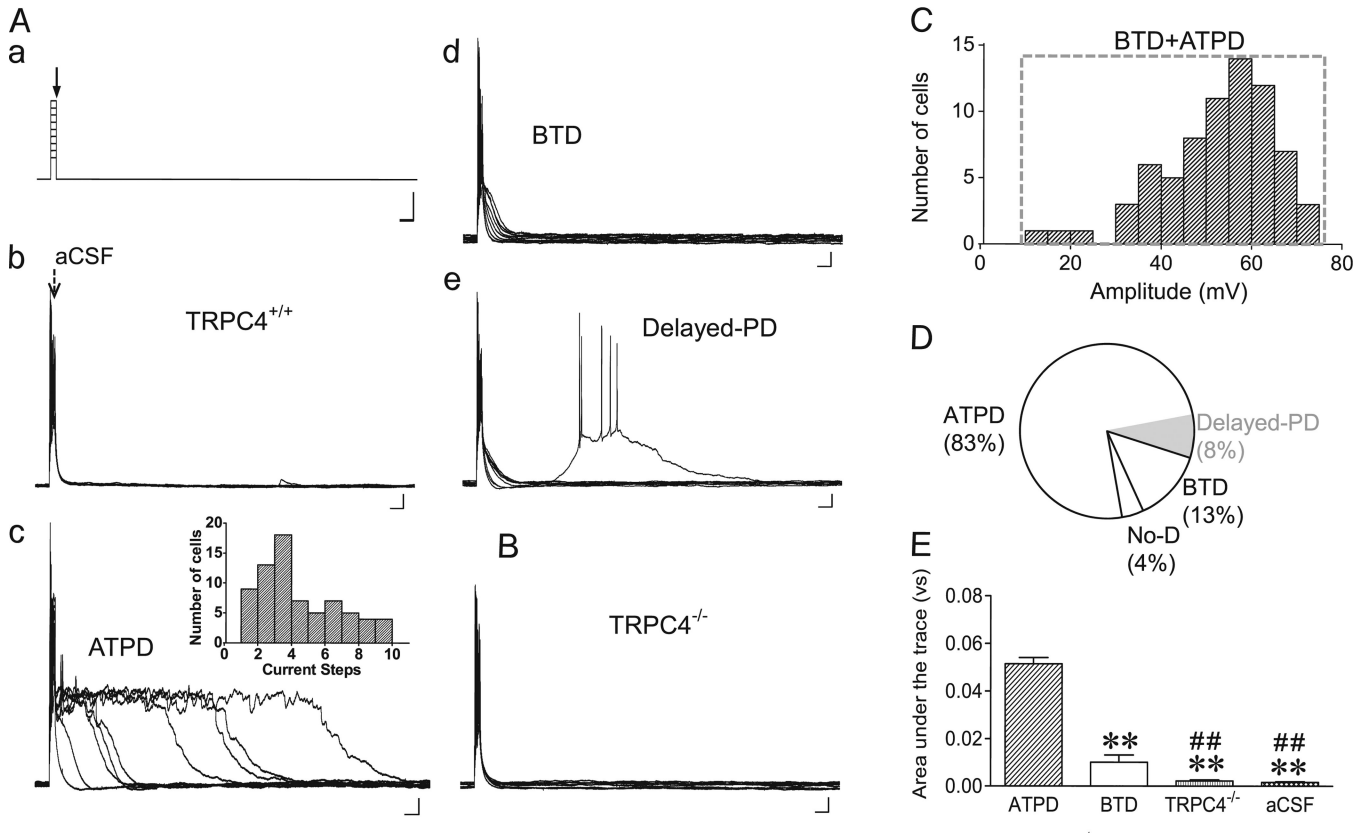

Fig. 4.

Current injection facilitates ATPD induction elicited by DHPG. *A*, Current clamp protocol (*a*) and representative traces of membrane potential changes elicited by ejecting aCSF (*b*) or 30 μM DHPG (*c*–*e*) onto WT LS neurons held initially at −80 mV. A current injection (20 ms, 0.2–1 nA, with a 0.1-nA increment) was applied immediately before initiation of ejection (5–20 psi, 30 ms) (CC-80s). Traces from all nine sweeps are overlaid. Current injection alone (with aCSF ejection) only elicited burst firing within the 20-ms injection period and the recovery of membrane potential to the pre-injection level was very quick (*b*). With ejection of DHPG, ATPD (*c*), BTD (*d*), and delayed-PD (*e*) were evoked in certain but not necessarily all sweeps. Note the maximal ATPD, as determined by area under the trace, could occur at any sweep (*c*, *inset*). *Scale bars*: 50 ms, 300 pA (*a*); 50 ms, 10 mV (*b*–*e*). *B*, Similar to *Ac*, but with a TRPC4$^{-/-}$ neuron. Neither BTD nor ATPD was evoked in TRPC4$^{-/-}$ LS neurons. C, Distribution of peak depolarization amplitude evoked by current injection plus DHPG ejection at CC-80 for TRPC4$^{+/+}$ LS neurons. *D*, Pie chart for the proportions of TRPC4$^{+/+}$ LS neurons that showed ATPD, BTD and no depolarization (No-D) with the CC-80s protocol. Delayed-PD was found in some ATPD neurons. *E*, Summary of maximal depolarization response, as determined by area under the trace from the sweep with the longest depolarization period and shown as mean±SEM, for TRPC4$^{+/+}$ neurons recorded with the CC-80s protocol and with DHPG (ATPD: n=62, BTD: n =10,) or aCSF (n =7) ejection and for TRPC4$^{-/-}$ neurons with DHPG ejection (n=9). **P<0.01, compared to ATPD; $^{\#\#}P$ <0.01, compared to BTD

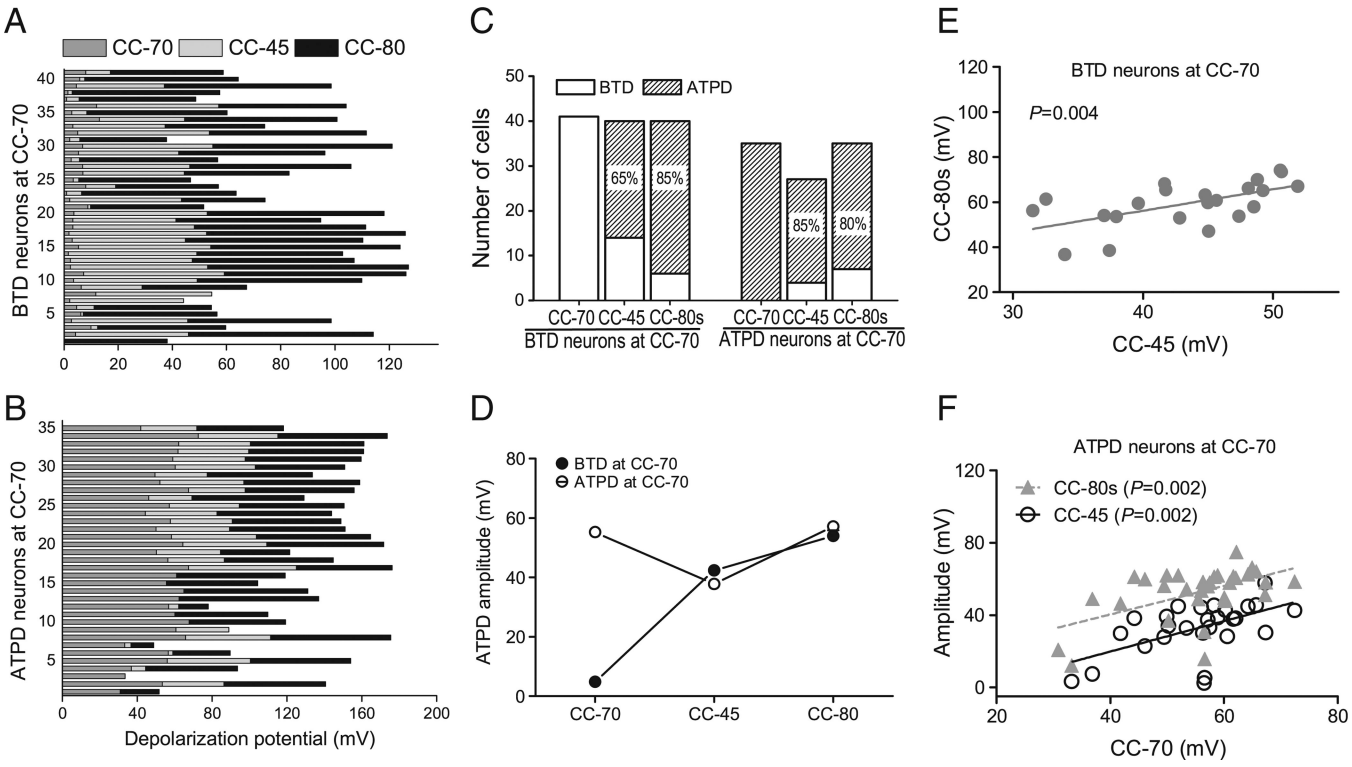

Fig. 5.

Transformations between BTD and ATPD and correlations of membrane potential changes under different recording conditions. *A*, Stacked bar graph showing peak depolarization amplitudes elicited by 30 μM DHPG sequentially using the CC-70, CC-45, and CC-80s protocols for individual neurons that showed BTD at CC-70. *B*, The same analysis as in *A*, but for individual neurons that showed ATPD at CC-70. *C*, Stacked bar graphs showing the total number of BTD and ATPD cells under the three recording conditions. Cells are grouped according to their responses at CC-70 as either BTD (*left*) or ATPD (*right*) and the proportions of ATPD cells at CC-45 and CC-80s in each group are indicated. *D*, Average peak depolarization amplitude of ATPD neurons at CC-45 and CC-80s with the cells grouped according to their responses at CC-70. Note the CC-70 BTD and ATPD neurons had similar levels of depolarization when transformed to ATPD at CC-45 or CC-80s. The average ATPD amplitudes are similar between CC-70 and CC-80s. *E*, Correlation of peak depolarization amplitudes recorded at CC-45 and CC-80s for neurons that showed BTD at CC-70. *F*, Correlation of peak depolarization amplitudes recorded between CC-70 and CC-45 and that between CC-70 and CC-80s for neurons that showed ATPD at CC-70. *E* and *F* highlight the potential common mechanism that underlies the induction of ATPD despite the remarkable differences among individual LS neurons

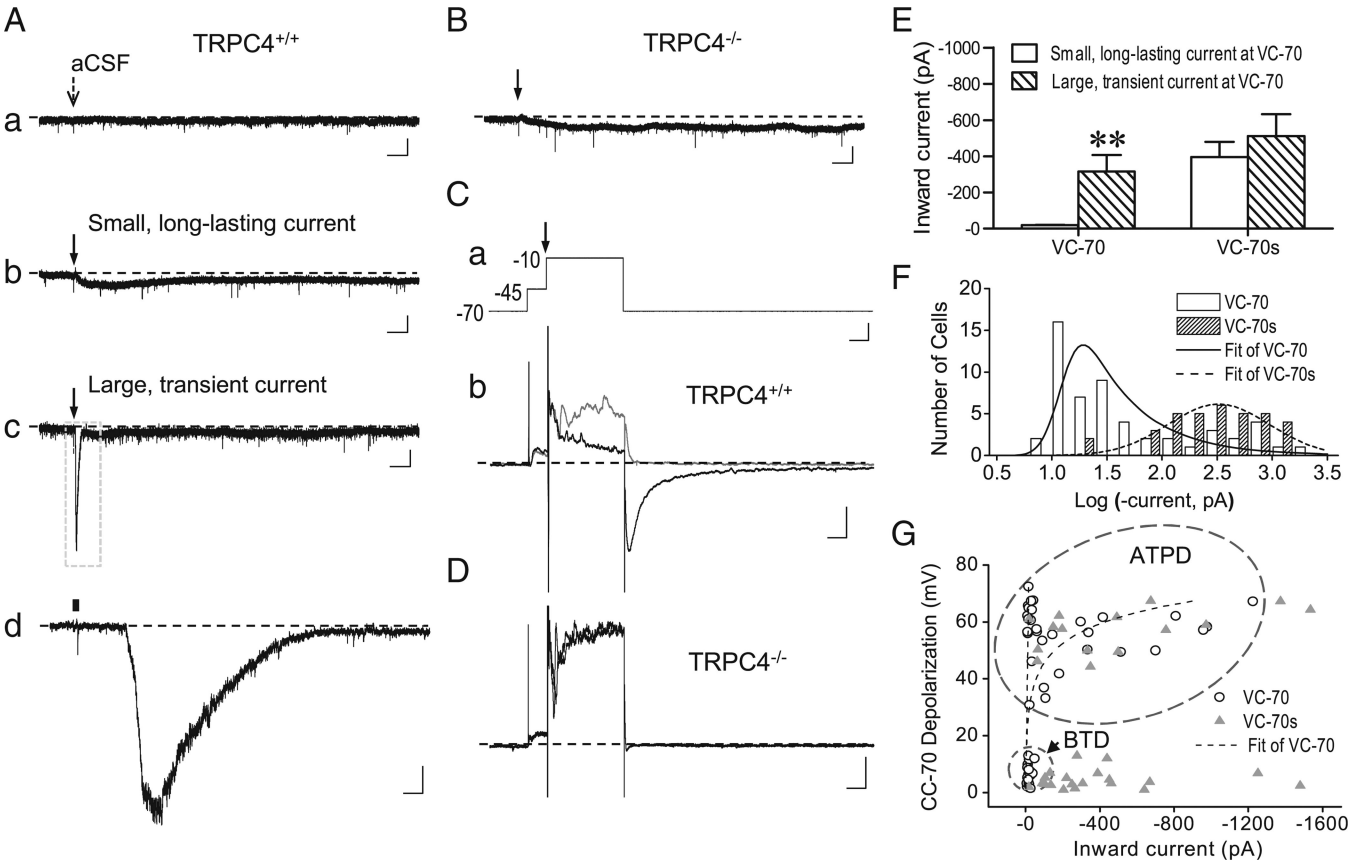

Fig. 6.

DHPG-evoked inward current in LS neurons. *A*, Representative traces showing changes in membrane current elicited by ejecting aCSF (*a*) or 30 μM DHPG (*b–d*) onto WT LS neurons voltage clamped at −70 mV (VC-70). DHPG evoked either small, long-lasting (*b*) or large, transient current (*c*, *d*). *Arrows* (*a–c*) indicate the time of ejection (5–20 psi, 30 ms). *d*, The boxed area in *c* in expanded scales, with the ejection period indicated by the *black bar*. *Scale bars*: 3 s, 50 pA (*a–c*); 100 ms, 50 pA (*d*). *B*, Similar to *Ab*, but for a TRPC4$^{-/-}$ LS neuron. Only small and slowly developing currents were elicited by DHPG ejection in TRPC4$^{-/-}$ LS neurons. *C*, Effect of depolarizing voltage steps on inward current elicited by DHPG ejection. *a*, Voltage protocol used for VC-70s, with the time of ejection indicated by the *arrow* (*top*, *scale bars*: 50 ms, 20 mV). *b*, Representative current traces for TRPC4$^{+/+}$ LS neurons that received only voltage steps (*gray*) or voltage steps plus DHPG ejection (*black*). *Scale bars*: 50 ms, 200 pA. *D*, Similar to *Cb*, but for a TRPC4$^{-/-}$LS neuron. Note the nearly complete overlap between *gray and black* traces. *E*, Average (mean±SEM) peak inward current amplitude evoked by VC-70 and VC-70s protocols in TRPC4^{++} neurons, grouped according to the response at VC-70 as either small, long-lasting or large, transient current. For VC-70s, the amplitude was measured at the peak of tail current after returning to −70 mV. Note the marked difference between small (n =22) and large current (n =32) by the VC-70 recordings; however, with the VC-70s protocol, similar peak amplitudes were obtained no matter if the neurons had small (n =20) or large (n = 15) current at VC-70. **P<0.01, compared to small current group at VC-70. *F*, Distribution of peak current

amplitudes evoked at VC-70 and VC-70s for TRPC4$^{+/+}$ neurons. Note the right shift for VC-70s. *G*, Correlation between DHPG-evoked inward currents and membrane depolarization at −70 mV Note neurons that displayed BTD (*circled area*) at CC-70 only developed small current at VC-70, but large inward currents were evoked at VC-70s regardless whether the neurons showed BTD or ATPD (*oval area*) at CC-70

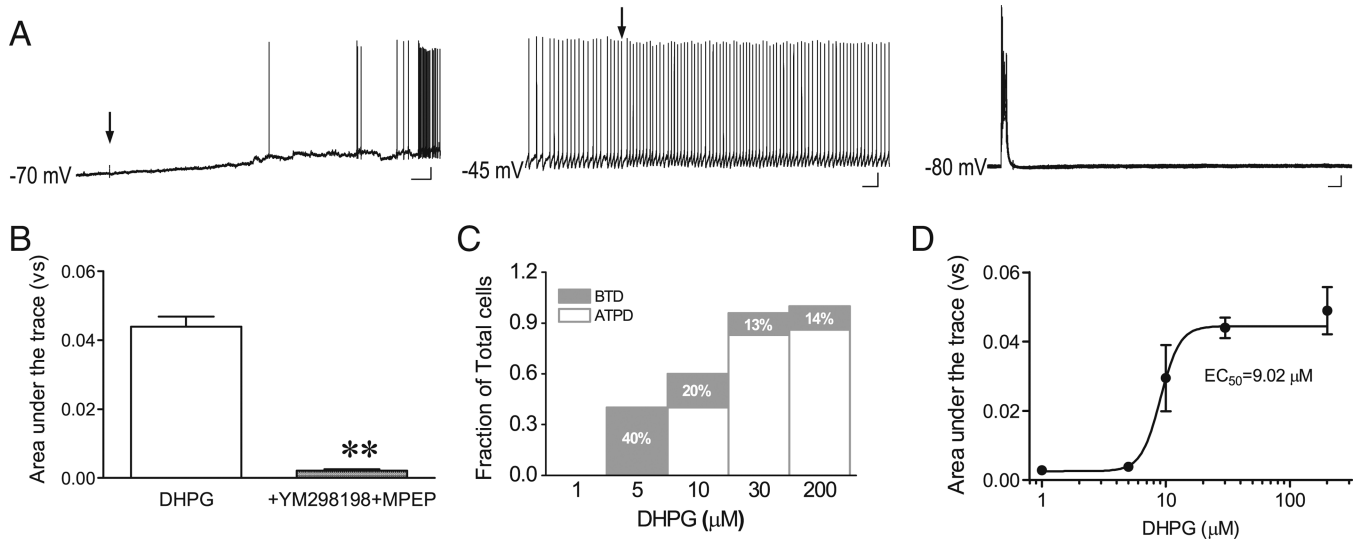

Fig. 7.

ATPD induction in LS neurons is dependent on DHPG concentration and mediated by group I mGluRs. *A*, representative traces showing blockage of ATPD induction by 30 μM YM298198 plus 10 μM MPEP ejected together with 30 μM DHPG to an LS neuron in all three current clamp conditions. *Arrows* indicate the time of drug ejection (5–20 psi, 30 ms). *Scale bars*: 3 s, 10 mV for CC-70; 0.5 s, 10 mV for CC-45, 50 ms, 10 mV for CC-80s. *B*, Quantification based on area under the trace for the sweep with the largest depolarization at CC-80s. Shown are means±SEM for DHPG-evoked depolarization in the absence (n =75) or presence of YM298198 and MPEP (n =6). $^{**}P$ <0.01, compared to DHPG alone. *C*, Stacked bar graph showing proportions of LS neurons that showed BTD and ATPD in response to the CC-80s protocol at different DHPG concentrations. The remaining neurons did not respond to the stimulation. *D*, Concentration–response curve of DHPG-induced membrane depolarization at CC-80s. Quantification was as in *B*; n =7, 6, 5, 75, and 7 for 1, 5, 10, 30, and 200 μM DHPG, respectively. For 30 μM DHPG, the same data as in *B* are shown

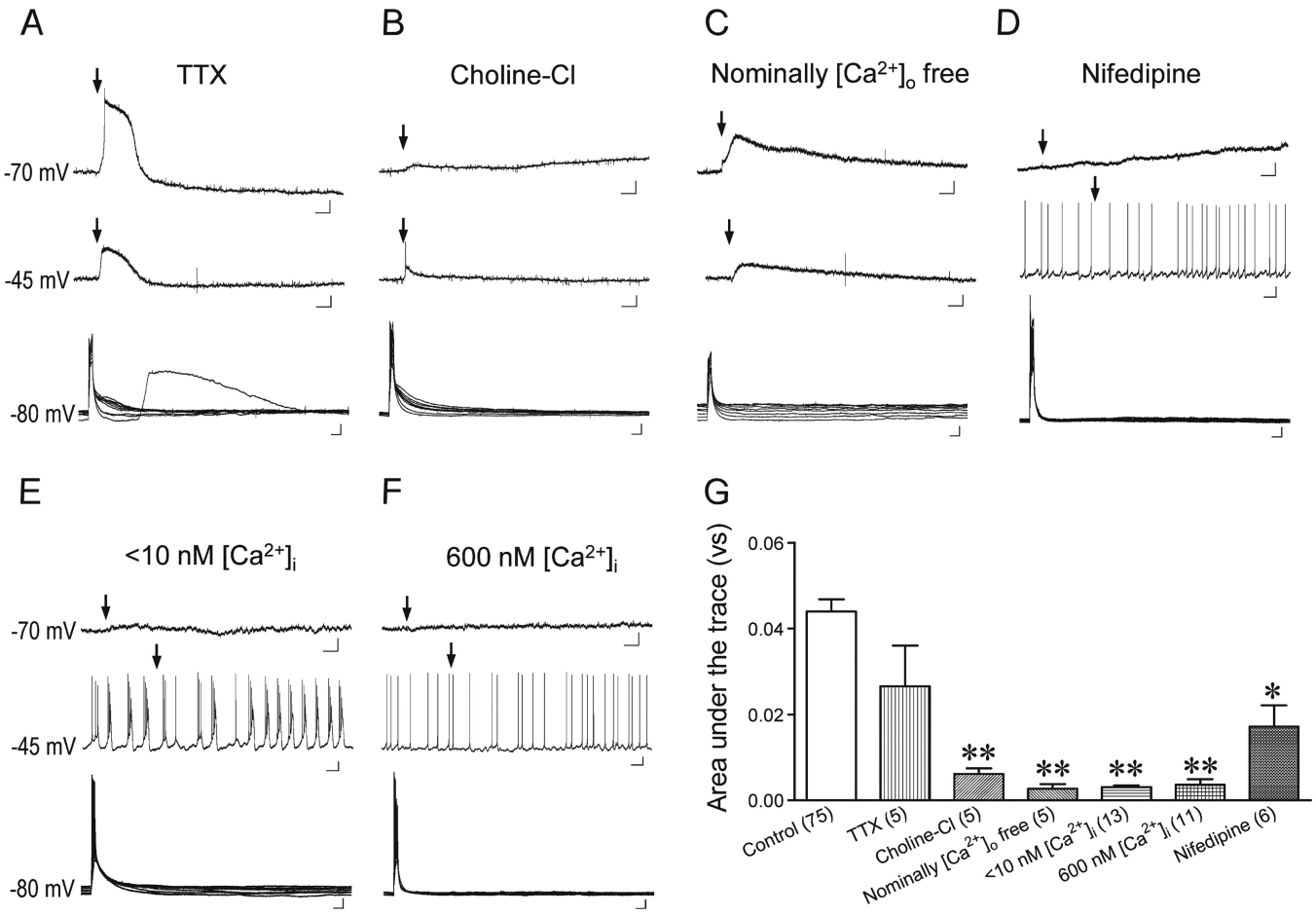

Fig. 8.

Effects of Na^+ and Ca^{2+} influx as well as dynamic changes of intracellular Ca^{2+} on DHPG-evoked ATPD induction in LS neurons. *A–F*, Representative traces of membrane potential changes in LS neurons in all three current clamp conditions with the aCSF containing 1 μM TTX to block voltage-gated Na^+ channels (*A* and *C*), substitution of NaCl in aCSF by choline-Cl to reduce Na^+ influx (*B*), omission of 2 mM $CaCl_2$ from aCSF to prevent Ca^{2+} influx (*C*), block of L-type Ca^{2+} channels by nifedipine (30 μM, ejected together with DHPG) (*D*), substitution of 0.05 mM EGTA by 10 mM BAPTA in the patch pipette solution to prevent intracellular Ca^{2+} rise (*E*, free $[Ca^{2+}]_i$ <10 nM), or substitution of 0.05 mM EGTA by 10mMBAPTA plus 7.24mM$CaCl_2$ in the pipette solution to provide an elevated intracellular Ca^{2+} concentration (free $[Ca^{2+}]_i$ ~600 nM) but prevent it from fluctuating (*F*). Note, ATPD was still induced in the presence of TTX, which eliminated all action potentials, but was blocked under all other conditions. *Arrows and scale bars* are the same as in Fig. 7(A). *G*, Summary (mean±SEM) of DHPG-evoked depolarization at CC-80s under conditions shown in *A–F*. Quantification was as in Fig. 7(B); the numbers of neurons recorded are shown in parentheses. **P* <0.05, ***P* <0.01, compared to control (normal aCSF and ejection with DHPG alone, the same data as used in Fig. 7(B))

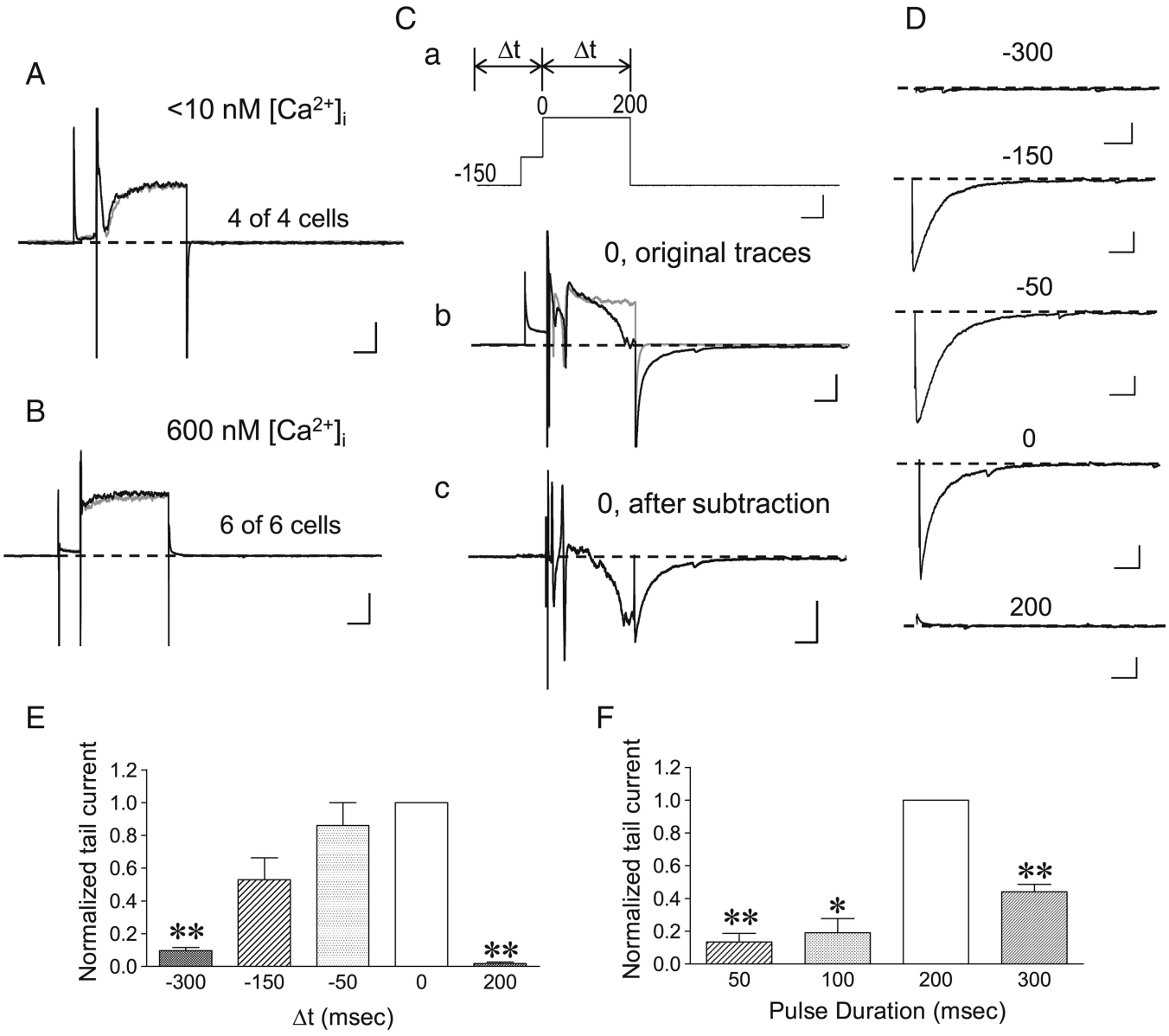

Fig. 9.

Dependence on intracellular Ca^{2+} dynamics and temporal relationship between mGluR stimulation and membrane depolarization of TRPC4-cc activation in LS neurons. *A*, *B*, Representative traces showing that DHPG ejection failed to evoke the tail current normally seen with the VC-70s protocol as shown in Fig. 6(Cb), when intracellular free Ca^{2+} concentration ($[Ca^{2+}]_i$) was buffered to either <10 nM (*A*) or ∼600 nM (*B*) by 10 mM BAPTA. The *gray traces* show responses to the voltage steps (same as in Fig. 6(Ca)) only, while the *black traces* display responses to the voltage steps with DHPG ejection. Note the near complete overlaps between the gray and black traces. *Scale bars*: 50 ms, 500 pA. C–E, Temporal relationship between mGluR stimulation and the depolarization step to −10 mV. *C*, Representative traces showing the VC-70s protocol and varying time intervals (Δ*t*) set in between the initiation of DHPG ejections (all 30 μM for 30 ms, 5–20 psi) and the start of the

200-ms depolarization step to −10 mV (*a*), the responses of a WT LS neuron to the voltage protocol alone (*b*, *gray trace*) and the voltage protocol with DHPG ejection at Δ*t* =0 (*b*, *black trace*), and the subtraction between the two traces in *b* (*c*). Numeric labels in *Ca* indicate milliseconds. *Scale bars*: 50 ms, 20 mV for *a*, 50 ms, 500 pA for *b* and *c*, *D*, Representative traces showing the subtracted tail currents, as in *Cc*, elicited by the VC-70s protocol with varying Δ*t* as indicated (in milliseconds). For clarity, current responses during voltage steps were omitted. Records in *C* and *D* were from the same cell. *Scale bars*: 50 ms, 200 pA. *E*, Summary data of tail current amplitudes normalized to that of Δ*t* =0, for conditions shown in *C* and *D*. *n* =3–5, ***P* <0.01, compared to Δ*t* =0 by paired *t* test. *F*, Similar to *E* with Δ*t* =0, but varying step durations to −10 mV were used. Summary data of tail current amplitudes normalized to that of the 200-ms step. *n* =3–5, **P* <0.05, ***P* <0.01, compared to 200 ms by paired *t* test